Synaptic vesicles that store monoamines and glutamate differ in protein composition.

Hrach Asmerian[1*], Alexia J. Diaz[1*], Hongfei Xu[2], Juan A. Oses-Prieto[3], Jacob Alberts[1], Anna Sanetra[1], Barathan Gnanabharathi[1], Noah Carr[1], Alma L. Burlingame[3], Robert H. Edwards[2], Kätlin Silm[1#]

Author affiliations:

[1]Center for Neural Science and Medicine, Board of Governors Regenerative Medicine Institute, Departments of Biomedical Sciences and Neurology, Cedars-Sinai Medical Center, Los Angeles, CA, USA.

[2]Departments of Physiology and Neurology, University of California, San Francisco School of Medicine, San Francisco, CA, USA.

[3]Department of Pharmaceutical Chemistry, University of California, San Francisco School of Medicine, San Francisco, CA, USA.

[#]Corresponding author: Katlin Silm, Katlin.silm@cshs.org

*Equal contribution

ABSTRACT

Neuromodulators such as the monoamines are known to differ from classical neurotransmitters like glutamate in the time scale of signaling due to activation of slower G protein-coupled receptors. Recent work has suggested that the mode of release also differs between classical and modulatory transmitters. Although many components of neurotransmitter release machinery have been identified, we still understand little about the mechanisms responsible for differences in release. In this study, we address the differences between release of dopamine and glutamate by comparing the composition of synaptic vesicles (SVs) that contain the vesicular monoamine transporter 2 (VMAT2) versus vesicular glutamate transporter 2 (VGLUT2). Previous work has shown that these SV populations differ in frequency dependence, recycling kinetics and biogenesis. Taking advantage of a CRISPR-generated knock-in mouse with a cytoplasmic hemagglutinin (HA) tag at the N-terminus of VMAT2 to immunoisolate monoamine SVs, we find differences in the abundance and isoform expression of many SV protein families. Validation in primary neurons and in brain tissue confirms these differences in SV protein abundance between dopamine and glutamate release sites. Functional analysis reveals that the loss of differentially

35 expressed SCAMP5 selectively impairs the recycling of VGLUT2 SVs, sparing VMAT2 vesicles
36 in the same neuronal population. These findings provide new insights into the molecular diversity
37 of SVs and the mechanisms that regulate the release of dopamine and glutamate, with
38 implications for the physiological role of these transmitters and behavior.
39
40 **INTRODUCTION**
41
42 Considerable work over decades has elucidated the basic machinery of neurotransmitter
43 release[1–3] but many questions remain about the molecular mechanisms that account for the
44 diversity in release properties at different synapses. Differences in release have been observed
45 between neuronal populations, but also individual release sites made by the same axon, and even
46 between vesicles in the same terminal[4–12]. This points to contribution from cell-wide differences
47 in the expression of synaptic proteins[13–16] but also to local mechanisms at synaptic sites, which
48 can be further modulated by postsynaptic neurons[4,6,8,10,17]. Furthermore, most of our
49 understanding of neurotransmitter release derives from work conducted in neurons that use fast,
50 synaptic signaling. In contrast to classical transmitters like glutamate and GABA which activate
51 ionotropic receptors, neuromodulators such as monoamines are often released at sites without a
52 direct postsynaptic target[18] and activate G-protein coupled receptors which signal over longer
53 times scales[19]. Despite critical roles in normal brain function, the molecular regulation of the
54 release of dopamine and other modulatory monoamine transmitters remains poorly understood.
55
56 While dopamine neurons fire tonically at low frequencies, dopamine release is significantly
57 increased during high frequency burst firing, and this is central to reinforcement learning[20]. This
58 property of dopamine release requires the recruitment of synaptic vesicles (SVs) specifically at
59 high frequency. Indeed, it has been shown that dopamine release is more loosely coupled to Ca^{++}
60 entry than fast synaptic release[21,22], consistent with a lower probability of release in response to
61 isolated stimuli, and a large increase with the accumulation of presynaptic Ca^{++} at high frequency.
62 Recent evidence also suggests that dopamine is only released from a subset of axonal
63 varicosities[23], which could reflect the sparsity of active zones in dopamine axons[24–26]. These
64 findings suggest that the machinery for release in dopamine neurons differs from the standard
65 model at classical synaptic sites.

66 Beyond the cell type specific features of dopamine axons, recent work in neurons that release
67 both dopamine and glutamate has shown that the two transmitters differ in release even from the

68 same neuron[22]. This is mediated by their storage in functionally distinct SVs that differ in synaptic
69 recycling kinetics and in frequency dependence of fusion, which leads to faster depression of
70 glutamate release[22]. Indeed, the formation of SVs that store monoamines relies heavily on a
71 pathway that involves the adaptor protein complex 3 (AP-3)[22,27]. While previous work that
72 addressed the role of this adaptor in other neuronal populations found a minor effect on the SV
73 cycle[28,29], loss of AP-3 leads to a severe reduction in the synaptic recycling of pHluorin-tagged
74 vesicular monoamine transporter 2 (VMAT2)[22,27]. This defect in turn reduces dopamine release in
75 the dorsal striatum and is especially pronounced at high stimulation frequencies[27]. Indeed, these
76 results are compatible with observations from multiple studies demonstrating that AP-3-
77 dependent SVs preferentially fuse during high frequency activity[27,30,31]. Strikingly, the recycling of
78 the vesicular glutamate transporter 2 (VGLUT2) that mediates glutamate corelease in dopamine
79 neurons is not affected by the loss of AP-3[22,27,30,32–34]. This suggests that VGLUT2 is excluded
80 from AP3-dependent SVs and targets to a subpopulation of vesicles that likely form via the
81 classical AP2-dependent mechanism[29,35]. AP-3-independent vesicles also contribute to tonic
82 dopamine release during low levels of activity as demonstrated by the more modest effect of the
83 AP-3 knock-out on dopamine release with stimulation at low frequency[27]. Differential reliance of
84 VMAT2 and VGLUT2 on the AP-3 pathway was also shown to extend beyond neurons that
85 release multiple transmitters[12,27,30]. Compatibly with this model, VGLUT2-dependent glutamate
86 release is consistently found to have high initial probability and to undergo depression with
87 sustained activity[5,7,30,36,37]. The differential reliance on AP-3 suggests that differences in the
88 biogenesis of VMAT2$^+$ versus VGLUT2$^+$ SVs contribute to the differences in release, likely by
89 affecting SV composition.

90 Compositional diversity among SVs has previously been addressed by comparing vesicles that
91 store the principal fast excitatory and inhibitory transmitters glutamate and GABA[38]. This
92 comparison identified few differentially expressed proteins, suggesting a relatively uniform
93 composition of SVs across neuronal populations. In the present study, we focus on SV
94 populations that contain VMAT2 or VGLUT2 but also differ in biogenesis mechanism and release
95 properties.

96 **RESULTS**

97 **Proteome of VMAT2$^+$ and VGLUT2$^+$ synaptic vesicles**. Due to the limited reliability of VMAT2
98 antibodies, we used CRISPR to generate a knock-in mouse with a hemagglutinin (HA) tag at the
99 N-terminus of VMAT2 (Figure 1A)[39]. HA-VMAT2 signal detected via anti-HA antibodies is present

100 in the cell bodies of dopamine, norepinephrine and serotonin neurons (Figure S1A, S1C-D) as
101 well as in the axonal projections of monoamine neurons in the striatum (Figure 1A, S1B). In
102 cultured neurons, HA-VMAT2 displays punctate signal in the processes of TH-positive neurons
103 (Figure S1E). HA-tagged VMAT2 is therefore faithfully targeted in monoamine neurons.

104 To isolate the vesicle populations from the HA-VMAT2 KI mice, we used a standard differential
105 centrifugation procedure to extract synaptic vesicles from synaptosomes via osmotic lysis (Figure
106 1B)[30,40]. However, since VMAT2 SVs in dopamine neurons are reported to localize in non-synaptic
107 sites that may be excluded from synaptosomes[41], we also collected light membranes released
108 from axonal fragments contained in the supernatant of the P2 synaptosome pellet (Figure 1B).
109 SVs were further purified using a 5-25% glycerol gradient where the HA-VMAT2 peak appeared
110 in fractions corresponding to SV proteins (Figure 1C). Vesicles isolated from LP2 and P4 samples
111 were detected in similar fractions (Figure 1C). However, we do observe a shift in HA-VMAT2
112 signal towards lower fractions compared to VGLUT2, which is consistent with recent reports of
113 larger SVs in dopamine neurons[42] (Figure 1C). VMAT2 and VGLUT2 SVs were then
114 immunoisolated from gradient purified SVs using antibodies against VGLUT2 or the HA tag in
115 VMAT2 (Figure 1D). Both HA-VMAT2 and VGLUT2 showed significant enrichment in SV
116 populations isolated using their respective antibodies (Figure 1E).

117 To compare the protein composition of the two SV populations, we performed mass spectrometry
118 with isotopic labeling by tandem mass tags (TMT). We initially completed this experiment in whole
119 brain samples, which contain VMAT2 vesicles from all monoamine projections. Mass
120 spectrometry of these samples indicates that many classical SV proteins were more abundant in
121 the VGLUT2$^+$ vesicle population while VMAT2$^+$ SVs were enriched in orphan transporter Slc10A4,
122 which is expressed by cholinergic and aminergic neurons and has a role in dopamine
123 homeostasis[43] , and in dopamine β-hydroxylase (DBH), a luminal SV enzyme that converts
124 dopamine into norepinephrine (Figure 1F). We also found the enrichment of VGLUT3 in
125 monoamine vesicles, which is consistent with the presence of this glutamate transporter in
126 serotonin neurons where it mediates glutamate corelease[44]. While the detection of DBH and
127 Slc10A4 support the enrichment of monoamine vesicles by VMAT2 immunoisolation, many novel
128 proteins that showed enrichment in these vesicles, as well as VMAT2 itself, were detected in only
129 a subset of samples (Figure 1F). This presumably reflected the insufficient enrichment of this SV
130 population from a sample where monoamine vesicles are relatively sparse. We therefore repeated
131 the immunoisolation and subsequent analysis using striatal samples where the VMAT2$^+$ SVs are
132 more abundant due to the dense dopaminergic projection. Similarly to the whole brain, we find

133 that many canonical SV proteins that are thought to be ubiquitously expressed in all SVs, show
134 enrichment in VGLUT2 vesicles (summarized in Figure 1G-I). VGLUT2-enriched proteins include
135 neuroprotective chaperone cysteine string protein α (CSPα), the synaptophysin family
136 (synaptophysin, synaptogyrin1 and synaptoporin), as well as SCAMP4 and 5. We also find that
137 members of the synaptotagmin (syt) protein family, which includes the fast SV calcium sensors
138 syt1 and syt2, differ in abundance in the two SV populations. Specifically, VGLUT2+ SVs appear
139 enriched in the fast calcium sensor syt2 and in calcium insensitive syt12 that has been implicated
140 in a protein kinase A-dependent form of presynaptic plasticity[45–47]. The analysis of striatal samples
141 also revealed more proteins with high abundance in VMAT2+ SVs. These include inhibitory
142 SNARE proteins tomosyn-1 and -2 (stxbp5 and stxbp5l) that were shown to increase the barrier
143 for SV fusion, thereby lowering release probability[48,49]. We also find that VMAT2 vesicles contain
144 more of chaperone DNAJb6 that is implicated in protection against α-synuclein pathology[50,51] and
145 in juvenile-onset parkinsonism[52] as well as SCAMP2 that was shown to influence trafficking of the
146 dopamine transporter[53]. While many well-known SV proteins differ in localization to the two vesicle
147 populations, essential components of the release machinery such as VAMP2, SNAP25 and NSF
148 are present at comparable levels in VMAT2$^+$ and VGLUT2$^+$ SVs (Figure 1F, 1G). Similarly,
149 subunits of the *v*-ATPase show no consistent enrichment in either vesicle population in striatal
150 samples (Figure S2A).

151 In addition to classical SV proteins, we find the differential expression of several Rab proteins,
152 with Rab3 and Rab11b enriched in VGLUT2$^+$ SVs and Rab4 in the VMAT2$^+$ sample, which could
153 reflect trafficking of the two transporters via distinct endosomal compartments (Figure 1F, 1G).
154 Furthermore, we observe the more abundant association of VMAT2$^+$ SVs with dynactin and
155 dynein subunits, suggesting a differential requirement for retrograde axonal and anterograde
156 dendritic transport that would be consistent with the known release of monoamines from dendrites
157 as well as axons (Figure 1F, 1G)[54]. Since VMAT2 and VGLUT2 vesicles differ in reliance on
158 adaptor protein complexes for recycling from the plasma membrane, we also analyzed the data
159 for AP-2 and AP-3 subunit abundance in the two SV populations (Figure S2B). While AP-2
160 subunits are present at comparable levels in both vesicle populations, AP-3 components are
161 detected consistently only in whole brain samples where they associate preferentially with VMAT2
162 vesicles.

163 **Expression of SV proteins in primary dopamine and glutamate neurons**. To assess
164 differences in VMAT2$^+$ and VGLUT2$^+$ SV composition, we first used primary midbrain cultures
165 from HA-VMAT2 KI mice as these cultures contain both dopamine neurons and VGLUT2$^+$

166 glutamate neurons. To compare SV protein abundance in these neuronal populations, we
167 identified regions of interest (ROIs) based on the expression of HA-VMAT2 or VGLUT2 and
168 quantified the fluorescence intensity of candidate proteins in both sets of ROIs. Since VMAT2
169 localizes to the somatodendritic as well as axonal compartment[55], we also examined the
170 colocalization of HA-VMAT2 with the dendritic protein MAP2. We find a more diffuse HA-VMAT2
171 signal in MAP2$^+$ fibers, while the vast majority of bright punctate structures similar in size and
172 appearance to VGLUT2$^+$ varicosities localize to MAP2$^-$ axonal projections (Figure S3). These
173 results therefore compare axonal varicosities from the two neuronal populations. As predicted by
174 the proteomics results, orphan transporter Slc10A4[43] localizes to VMAT2$^+$ rather than VGLUT2$^+$
175 terminals (Figure 2A). In contrast, VGLUT2$^+$ sites contain more of the canonical SV protein
176 synaptophysin (Figure 2E, S4A) as well as the related synaptogyrin1 (Figure 2F, S4B). VGLUT2$^+$
177 terminals also contain more of presynaptic chaperone CSPα (Figure 2D) and SCAMP5 (Figure
178 2G, S4C). However, the SV SNARE protein VAMP2 occurs at similar levels in both release sites
179 (Figure 2H, S4D) supporting the specificity of differences for other proteins and arguing against
180 substantial differences in SV cluster size. For synaptophysin, synaptogyrin1, CSPα, SCAMP5 and
181 Slc10A4, the same trends in expression were consistently observed in all analyzed dopamine and
182 glutamate neurons, including fields of view that contain both dopamine and VGLUT2$^+$ glutamate
183 axons. However, the analysis of syt2 revealed that although syt2 signal in dopamine neurons was
184 consistently close to background, glutamate neurons fall into two populations: VGLUT2 neurons
185 with low or nonexistent syt2 signal similar to dopamine neurons, and another with strong syt2
186 expression that colocalizes with VGLUT2 (Figure 2C, 2I, 2J). These findings suggest a molecular
187 heterogeneity among the VGLUT2$^+$ glutamate neurons present in midbrain cultures. The other
188 fast calcium sensor syt1 occurs in both types of neurons, but its signal intensity in midbrain
189 cultures is consistently higher at dopamine release sites (Figure 2B).

190 To directly test whether dopamine and glutamate release sites differ in the copy number of SV
191 proteins, we quantified both VMAT2-enriched syt1 and VGLUT2-enriched CSPα in the same ROIs
192 (Figure 2K-N, S5). The ratio of syt1/CSPα is significantly higher in VMAT2$^+$ varicosities indicating
193 that individual dopamine release sites contain more syt1 and less CSPα than VGLUT2 terminals
194 (Figure 2M, 3N). These results support the differences in SV composition identified by mass
195 spectrometry and show that possible differences in SV cluster size in dopamine versus glutamate
196 neurons[42] cannot alone explain differences in SV protein abundance in VGLUT2 versus VMAT2
197 release sites.

198 **The composition of synaptic vesicles differs at dopamine and glutamate release sites in**
199 **the striatum**. To test the differential expression of SV proteins at dopamine and glutamate
200 release sites within the intact neural circuitry, we stained for candidate proteins in brain slices
201 from HA-VMAT2 KI mice and quantified their abundance in VMAT2$^+$ and VGLUT2$^+$ varicosities
202 (Figure 3, Figure S6). We focused on the striatum since it receives both dense dopamine
203 projections from the midbrain and VGLUT2$^+$ input from the thalamus. We acquired z-stacks and
204 used automatic segmentation to generate three-dimensional (3D) VGLUT2 and VMAT2 surfaces
205 followed by quantification of the mean fluorescence intensity for the proteins of interest within the
206 same image (Figure 3A). As predicted by the proteomics results and confirmed in primary culture,
207 Slc10A4 is enriched at dopamine release sites and colocalizes with VMAT2 (Figure 3B, 3C). If
208 combined with TH staining to differentiate dopamine release sites from cholinergic terminals,
209 which also express this transporter[56], Slc10A4 can serve as a reliable marker for dopamine
210 release sites. CSPα (Figure 3D, 3E), SCAMP5 (Figure S6A, S6B) and synaptophysin (Figure
211 S6C, S6D) are more abundant in VGLUT2$^+$ varicosities. As in primary cultures, the mean intensity
212 of VAMP2 signal was comparable in VGLUT2$^+$ and VMAT2$^+$ surfaces (Figure S6E, S6F).

213 Experiments in primary cultures indicated that syt2 is present in only a subset of VGLUT2$^+$
214 neurons (Figure 2I). We stained for syt2 in multiple brain regions that receive VGLUT2$^+$
215 projections to determine whether VGLUT2$^+$ glutamate neurons in different structures differ in
216 expression of syt2 (Figure 4). We focused on the striatum, CA2 region of the hippocampus, and
217 the posterior thalamic nucleus (PO), dorsal lateral geniculate nucleus (DLG) and ventral posterior
218 nucleus (VPN)[57]. We observed HA-VMAT2$^+$ fibers in all these structures, enabling us to compare
219 the fraction of VMAT2$^+$ and VGLUT2$^+$ varicosities that contain syt2 as well as to compare syt2
220 intensity at the two classes of release site. VMAT2$^+$ and VGLUT2$^+$ varicosities were considered
221 syt2$^+$ if 40% of their volume overlapped with syt2 labeling (Figure 4A). Since none of the three
222 presynaptic proteins are expressed by all neurons, the labeling density in all brain regions was
223 sufficiently low to assess the extent of overlap without significant contribution of signal from
224 adjacent structures (Figure 4B, 4C). We find that although syt2 signal is very low in VGLUT2$^+$
225 terminals of the striatum and in region CA2 of the hippocampus, it is abundant at the majority of
226 VGLUT2$^+$ release sites in thalamic nuclei and absent from the majority of VMAT2$^+$ varicosities in
227 all structures (Figure 4B-D). When we quantified the mean intensity of syt2 signal in monoamine
228 and glutamate release sites across all regions, we find that this calcium sensor is significantly
229 more abundant in VGLUT2 varicosities in the DLG that contains the large VGLUT2$^+$ terminals of
230 retinal ganglion cells[58] (Figure 4B, 4C, 4E) and in the VPN where VGLUT2-dependent glutamate

231 release relays sensory information from the spinal cord and brain stem[59] (Figure 4E). Mean syt2
232 intensity was not significantly different between VMAT2$^+$ and VGLUT2$^+$ varicosities in the striatum,
233 CA2 and PO. These results confirm the differences in composition of VMAT2$^+$ and VGLUT2$^+$ SVs
234 identified by the proteomics.

235 **SV protein composition of VGLUT2+ release sites in dopamine neurons differs from**
236 **VMAT2-only varicosities**. The corelease of glutamate by midbrain dopamine neurons raises the
237 possibility that SVs that store dopamine and glutamate may differ within the same population of
238 neurons. We previously found that the exocytosis and recycling of VGLUT2$^+$ SVs in cultured
239 dopamine neurons occurs with faster kinetics than VMAT2$^+$ SVs[22], indicating differences in the
240 mode of release in the same cell. Glutamate release from coreleasing neurons also differs from
241 dopamine release in short-term plasticity[22]. If VGLUT2$^+$ and VMAT2$^+$ SVs in dopamine neurons
242 indeed differ in protein content, it should result in altered presynaptic composition in VGLUT2$^+$
243 release sites in dopamine neurons compared to VMAT2-only sites.

244 The corelease of glutamate with dopamine reflects the expression of VGLUT2 by a subset of
245 midbrain dopamine neurons[32,33]**.** To investigate the localization of VMAT2 and VGLUT2 in these
246 cells, we again took advantage of midbrain cultures from HA-VMAT2 mice (Figure 5). We find that
247 within TH$^+$ neurons that label for both VMAT2 and VGUT2, most release sites contain detectable
248 signal for both transporters, even though the relative intensities vary (Figure 5A-C). While VMAT2
249 signal is comparable in release sites of VMAT2-only and VMAT2$^+$/VGLUT2$^+$ neurons, VGLUT2
250 abundance in presynaptic varicosities of cultured VMAT2$^+$/VGLUT2$^+$ neurons is significantly lower
251 than in glutamate-only cells (Figure 5D). This suggests a lower VGLUT2 copy number per vesicle
252 or its presence on a subset of vesicles within coreleasing terminals.

253 We also determined whether VMAT2$^+$/VGLUT2$^+$ sites differ from VMAT2-only varicosities in the
254 expression of other SV proteins. We find that VMAT2-enriched Slc10A4 and equally distributed
255 VAMP2 are present at similar levels in VMAT2-only and VMAT2$^+$/VGLUT2$^+$ boutons (Figure 5G-
256 H). Likewise, the abundance of SV calcium sensors syt1 and syt2 is not affected by the presence
257 of VGLUT2 at VMAT2 sites (Figure 5I-J). However, CSPα, SCAMP5 and synaptophysin are
258 significantly more abundant at VMAT2$^+$/VGLUT2$^+$ boutons compared to VMAT2-only SV clusters
259 (Figure 5E, 5F, 5K-M). Furthermore, we find that the abundance of Slc10A4 measured in
260 individual release sites of coreleasing neurons correlates better with VMAT2 than VGLUT2
261 abundance at the same varicosities (Figure 5N). Conversely, synaptophysin signal correlates with
262 VGLUT2 expression (Figure 5O) supporting the preferential targeting of synaptophysin to

263 VGLUT2 SVs. Altogether, we find that VGLUT2$^+$ presynaptic varicosities in dopamine neurons
264 resemble typical glutamate release sites pointing to a distinct composition of VGLUT2 SVs within
265 dopamine neurons.

266 **SVs containing VGLUT2 and VMAT2 segregate within presynaptic varicosities of**
267 **dopamine/glutamate coreleasing neurons**. VMAT2 and VGLUT2 colocalize at the majority of
268 release sites made by cultured dopamine neurons, but previous work using heterologous
269 reporters has suggested that they may localize to distinct SVs at these sites[22]. We have now
270 addressed this question using endogenous proteins. Since classical confocal microscopy does
271 not allow us to resolve SVs within a single presynaptic bouton, we thus took advantage of the
272 Nikon Spatial Array Confocal (NSPARC) technology to access enhanced spatial resolution
273 compared to classical confocal detection systems[60]. We focused on individual presynaptic
274 varicosities that contain TH, HA-VMAT2 and VGLUT2 to evaluate the degree of colocalization
275 between VMAT2 and VGLUT2 signal within the release site and to investigate the colocalization
276 of the signal for the transporters and differentially expressed SV proteins (Figure 6). First, we
277 compared the colocalization of HA-VMAT2 and VGLUT2 (Figure 6B, 6C), using HA signal stained
278 with two secondary antibodies coupled to different fluorophores as control (Figure 6A). As
279 expected, HA signal detected in two channels shows a high degree of colocalization. We also
280 detect substantial overlap between HA-VMAT2 and VGLUT2 signal, however, it is significantly
281 lower compared to the control condition comparing HA signal in two channels (Figure 6A). Since
282 we detect a partial segregation of VMAT2 and VGLUT2 into different structures within presynaptic
283 varicosities, we compared the correlation of VGLUT2-enriched synaptophysin and VMAT2-
284 enriched syt1 with the signal for the two transporters. We find that synaptophysin fluorescence
285 correlates more with VGLUT2 than VMAT2 in presynaptic terminals that contain both transporters
286 (Figure 6B) while syt1 signal displays similar correlation with both VGLUT2 and VMAT2 (Figure
287 6C). These results suggest that VGLUT2 targets to an SV population with distinct composition.

288 **Loss of SCAMP5 selectively impairs the synaptic recycling of VGLUT2 vesicles**. If VGLUT2
289 and VMAT2 SVs differ in composition even in the same neuronal population, then elimination of
290 a differentially expressed protein should preferentially affect the synaptic recycling of vesicles
291 expressing more of that protein. We focused on SCAMP5 as we have validated its significantly
292 higher abundance on VGLUT2 vesicles and previous studies have shown that its loss of function
293 affects the SV cycle and neurotransmitter release[61,62]. To address its role in the release of
294 VMAT2$^+$ versus VGLUT2$^+$ vesicles, we took advantage of the pHluorin reporter that enables
295 monitoring the properties of the SV cycle when fused to luminal domains of SV proteins. PHluorin

296 fluorescence is quenched in resting, acidic SVs but increases as SV fusion exposes the vesicle
297 lumen to the neutral extracellular environment and decreases with endocytosis and vesicle
298 reacidification[63]. We have previously shown that pHluorin-tagged VMAT2 reliably targets to AP-
299 3-dependent SVs in both dopamine and hippocampal neurons whereas VGLUT2-pHluorin is
300 excluded from these vesicles[22,27]. To test whether the elimination of SCAMP5 has differential
301 effects on these SV pools, we used shRNA to knock down (KD) SCAMP5 expression (Figure 7).
302 Lentiviral delivery of a KD construct targeting SCAMP5 results in an efficient elimination of the
303 SCAMP5 protein from hippocampal neurons without affecting neuronal morphology or the
304 abundance of the SV calcium sensor syt1 (Figure 7A). To test the role of SCAMP5 in the VGLUT2$^+$
305 SV population, we infected neuronal cultures with VGLUT2-pHluorin together with a control
306 scrambled construct or SCAMP5 KD alone or in combination with an shRNA resistant rescue
307 construct. Neurons were stimulated for 60 seconds at 10 Hz. We find that the recycling of VGLUT2
308 SVs is reduced in the KD condition compared to a scrambled control but is restored to control
309 levels if SCAMP5 expression is rescued in the KD background (Figure 7B). The synaptic recycling
310 of AP-3-dependent SVs targeted by VMAT2-pHluorin is however not affected by the loss of
311 SCAMP5 (Figure 7C). These findings indicate that SCAMP5 is specifically involved in recycling
312 of vesicles that are enriched in VGLUT2 and despite its high abundance in the cell type, does not
313 have a detectable effect on the trafficking of the SV population targeted by VMAT2. Since the loss
314 of AP-3 does not completely abolish VMAT2 recycling[27], it remains possible that AP-3-
315 independent VMAT2$^+$ vesicles depend on SCAMP5 function but this effect is not detected due to
316 the abundance of VMAT2 on AP-3 SVs.

317 **DISCUSSION**

318 The results show that VMAT2$^+$ and VGLUT2$^+$ synaptic vesicles differ in protein composition.
319 VMAT2$^+$ vesicles contain fewer canonical SV proteins than VGLUT2$^+$ SVs but more of others.
320 These findings provide a basis to understand the different properties of monoamine release and
321 glutamate release that depends on VGLUT2.

322 We identify some of the same unique components of dopamine SVs that were detected in
323 previous studies that relied on synaptosome sorting or proximity labeling[16,26,64,65]. These include
324 putative transporters Slc10A4, VAT1 and SV2c[16,64,65]. While their substrate in dopamine neurons
325 and mechanism of action is not completely understood, the loss of Slc10A4 and SV2c leads to
326 reduced dopamine uptake into SVs and impaired release[43,66,67]. VAT1 was recently shown to bind

327 NADPH to function as a quinone oxidoreductase[68]. While its synaptic role in not known, its
328 enzymatic function could contribute to alleviation of oxidative stress.

329 The enrichment of Slc10A4 and SV2c in VMAT2+ SVs is likely explained by their high expression
330 in monoamine neurons and absence from many other neuronal populations[13–15]. However, we
331 also find differences in SV proteins that are expressed in most neurons. For example, VMAT2$^+$
332 SVs contain relatively little synaptophysin and closely related synaptogyrin1 and synaptoporin.
333 While the primary function of this protein family is not clear, their loss of function affects both
334 short- and long-term synaptic plasticity[69,70] as well as trafficking of other SV components[71–73].
335 Recent evidence also points to a role of this protein family in the maintenance of SV size, with
336 larger SVs observed in the absence of synaptophysin[74,75]. Furthermore, synaptophysin enables
337 the expansion of filling SVs, which accelerates their fusion[75]. Low synaptophysin abundance on
338 VMAT2$^+$ vesicles could therefore affect their function as well as morphology, which is consistent
339 with recent reports of larger and less uniform SVs in dopamine release sites[42].

340 Among other canonical SV proteins, we find that VMAT2$^+$ and VGLUT2$^+$ vesicles differ in
341 synaptotagmin isoforms. Dopamine release sites are enriched in the fast Ca^{++} sensor syt1 and
342 lack the closely related fast isoform syt2 that is abundant in a subset of VGLUT2$^+$ glutamate
343 neurons that relay sensory information in a highly reliable manner. Additionally, VMAT2$^+$ SVs are
344 enriched in syt5 and VGLUT2$^+$ SVs in syt12. Unlike previous studies[64,65], we do not find a
345 significant enrichment of syt17 in VMAT2$^+$ vesicles. However, functional data supports syt17
346 localization on endosomal organelles that differ from SVs[76,77] which could explain its enrichment
347 in dopamine synaptosomes and axons but not SVs. Abundance of syt1 on VMAT2$^+$ SVs is
348 consistent with recent work which shows that this Ca^{++} sensor is required for most dopamine
349 release[78,79]. While syt1 and syt2 share high structural and functional similarity, several studies
350 have reported faster kinetics and higher temporal precision of release mediated by syt2[47,80] even
351 though this was not seen in all synapses[81,82]. The function of syt1 and syt12 but not syt2 is also
352 modulated by protein kinases A and C – known regulators of presynaptic plasticity[45,46,83]. Further
353 investigation is therefore needed to elucidate whether the expression of different synaptotagmins
354 contributes to the distinct kinetics and plasticity of dopamine and glutamate release.

355 VMAT2$^+$ and VGLUT2+ SVs also differ in SCAMP isoforms. SCAMP4 and -5 are more abundant
356 on VGLUT2$^+$ vesicles and SCAMP2 is on VMAT2$^+$ SVs. Consistently with its role in monoamine
357 release sites, loss of SCAMP2 has previously been shown to impair the trafficking of the dopamine
358 transporter DAT and serotonin transporter SERT[53,84]. In the context of neurotransmitter release,

359 SCAMP5 has been studied in most detail with multiple roles identified at the presynaptic terminal.
360 Its loss of function was shown to reduce the quantal content of glutamate release by impairing
361 presynaptic targeting of the cation/H^+ exchanger NHE6[85] and to enhance synaptic depression via
362 impaired release site clearance and endocytosis[61,62] but it is unclear whether these roles are
363 common to all isoforms. Direct comparison of SCAMPs in dense core vesicle exocytosis suggests
364 that while knock-downs of all studied isoforms reduce the number of exocytotic events, they have
365 distinct effects on the latency of exocytosis and only SCAMP1 and -5 have additional effects on
366 transmitter uptake[86]. Differential enrichment of SCAMP isoforms on VMAT2$^+$ and VGLUT2$^+$ SVs
367 is therefore likely to have distinct effects on release. Indeed, we now demonstrate that the loss of
368 SCAMP5 impairs the release of VGLUT2$^+$ SVs without affecting the vesicles targeted by VMAT2
369 even in the same neuronal population. These findings demonstrate that differences in SV
370 composition confer distinct regulation to VMAT2$^+$ and VGLUT2$^+$ SVs, which in turn mediate the
371 release of dopamine and glutamate.

372 Beyond SV membrane proteins, we also find that VMAT2$^+$ vesicles contain less of the lipid-
373 anchored neuroprotective chaperone CSPα. CSPα contributes to the correct folding of the release
374 machinery and its loss of function leads to a rapid presynaptic degeneration[87], while a reduced
375 copy number impairs synaptic function more slowly[88]. The low expression of CSPα at dopamine
376 release sites could therefore increase dopamine neuron susceptibility to protein misfolding which
377 might in turn contribute to their vulnerability in Parkinson's disease. In addition to SV proteins, we
378 find that dynactin and dynein subunits are preferentially associated with VMAT2$^+$ SVs, as reported
379 before[16]. Association with the dynein motor could reflect anterograde trafficking of VMAT2 in
380 dendrites or a more dynamic nature of diffusely distributed SVs in dopamine axons[18,41], which in
381 turn could affect their availability for release[89,90].

382 Differences in the abundance of SV proteins that are widely expressed across neurons suggests
383 that the formation of VMAT2+ and VGLUT2+ SVs depends on distinct mechanisms that differ in
384 efficiency or selectivity of protein recruitment. Indeed, the reliance of VMAT2 but not VGLUT2 on
385 the AP-3 pathway is likely to contribute to differences in SV composition and release[12,22,27].
386 Previous analysis of whole brain SVs in WT versus AP-3 knock-out mice confirmed the reduced
387 expression of known AP-3 client proteins, including VAMP7 and identified new SV proteins that
388 depend on AP-3 function, including phospholipid flippase ATP8a1 and Slc35g2 – a transporter
389 with unknown function[30,91,92]. While the abundance of most classical SV proteins was not found
390 to be changed[30], AP-3-dependent vesicles only constitute a small fraction of the total SV pool at
391 most synapses, making it challenging to detect changes in the abundance of proteins that do not

392 rely exclusively on AP-3 function for SV targeting[31,93]. We expected to find enrichment of known
393 AP3-dependent proteins in VMAT2+ SVs, however, while Slc35g2 appears abundant in these
394 vesicles, VAMP7 and ATP8A1 do not differ in enrichment in the two SV populations and
395 surprisingly, AP-3-dependent zinc transporter ZnT3 is enriched in the VGLUT2$^+$ population. ZnT3
396 targeting is partially explained by its lack of expression in dopamine neurons and presence in a
397 small subset of VGLUT2$^+$ glutamate neurons[14], however, it remains unclear how it is packaged
398 onto vesicles together with VGLUT2 that does not rely on AP-3. Additional work is also needed
399 to elucidate the localization of AP-3-dependent proteins VAMP7 and VMAT2 in the presynaptic
400 terminal. Indeed, VAMP7 has established roles in endolysosomal organelles[94–96] in addition to
401 SVs[30,31,91,93] and could therefore reside in a partially separate vesicle population at the release
402 site[97]. Among proteins enriched in VGLUT2$^+$ SVs, SCAMP5 is known to interact with AP-2 and
403 this interaction is required for its role in release sites clearance[62]. Synaptophysin has been shown
404 not to depend on AP-3[92,94]. Furthermore, its association with other SV proteins can affect their
405 sorting[72,73] and can therefore contribute to generating differences in the composition of VMAT2$^+$
406 and VGLUT2$^+$ SVs. Indeed, the distribution of known AP-3 cargos in the two vesicle populations
407 shows that reliance on distinct cargo adaptors is likely not sufficient to generate the observed
408 differences in protein composition. Indeed, it is likely that cell type-specific differences in gene
409 expression, differential reliance on adaptors as well as sorting by association with other SV
410 proteins all contribute to establishing the distinct composition of VMAT2$^+$ and VGLUT2$^+$ SVs[98].

411 A significant role of distinct trafficking mechanisms is further highlighted by the analysis of
412 VGLUT2$^+$ dopamine neurons. We find that while HA-VMAT2 and VGLUT2 colocalize at most
413 release sites in cultured dopamine/glutamate cells, they often differ in abundance. VGLUT2$^+$
414 release sites in dopamine neurons also differ in SV protein composition from VMAT2-only sites
415 suggesting a distinct composition of VGLUT2$^+$ SVs. While the analysis of VMAT2-only and
416 VMAT2$^+$/VGLUT$^+$ sites mostly compares different cells and could reflect differences in gene
417 expression between coreleasing and dopamine-only neurons, super-resolution imaging reveals a
418 partial segregation of VMAT2 and VGLUT2 as well as co-enriched SV proteins in individual
419 presynaptic varicosities. These findings show that VMAT2 and VGLUT2 are packaged into
420 biochemically distinct vesicles in the same cell and even presynaptic terminal. The specific effect
421 of SCAMP5 KD on VGLUT2$^+$ vesicles further demonstrates that differences in SV composition
422 translate into distinct regulation of release.

423 Targeting of VMAT2 and VGLUT2 to distinct vesicles is compatible with previous work, which
424 demonstrated the different kinetics and frequency dependence of dopamine and glutamate

425 release from coreleasing neurons[22]. However, glutamate corelease was also shown to affect
426 dopamine packaging into SVs via vesicular synergy, which would require at least a partial
427 coexistence of VMAT2 and VGLUT2 on the same vesicle[32]. Indeed, recent findings show that
428 while AP-3 is important for generating VMAT2$^+$ vesicles, the loss of this adaptor does not
429 completely abolish dopamine release[27]. This suggests that some VMAT2 localizes to AP-3-
430 independent SVs, which likely also contain VGLUT2. It is therefore possible that colocalization of
431 the transporters on the AP-3-independent SV pool drives vesicular synergy observed between
432 the two transmitters[32].

433 In summary, we elucidate the distinct molecular composition of monoamine and VGLUT2$^+$
434 glutamate SVs. The differential role of SCAMP5 illustrates the functional significance of these
435 differences. Other differentially expressed SV proteins presumably contribute to differences in
436 dopamine and glutamate release.

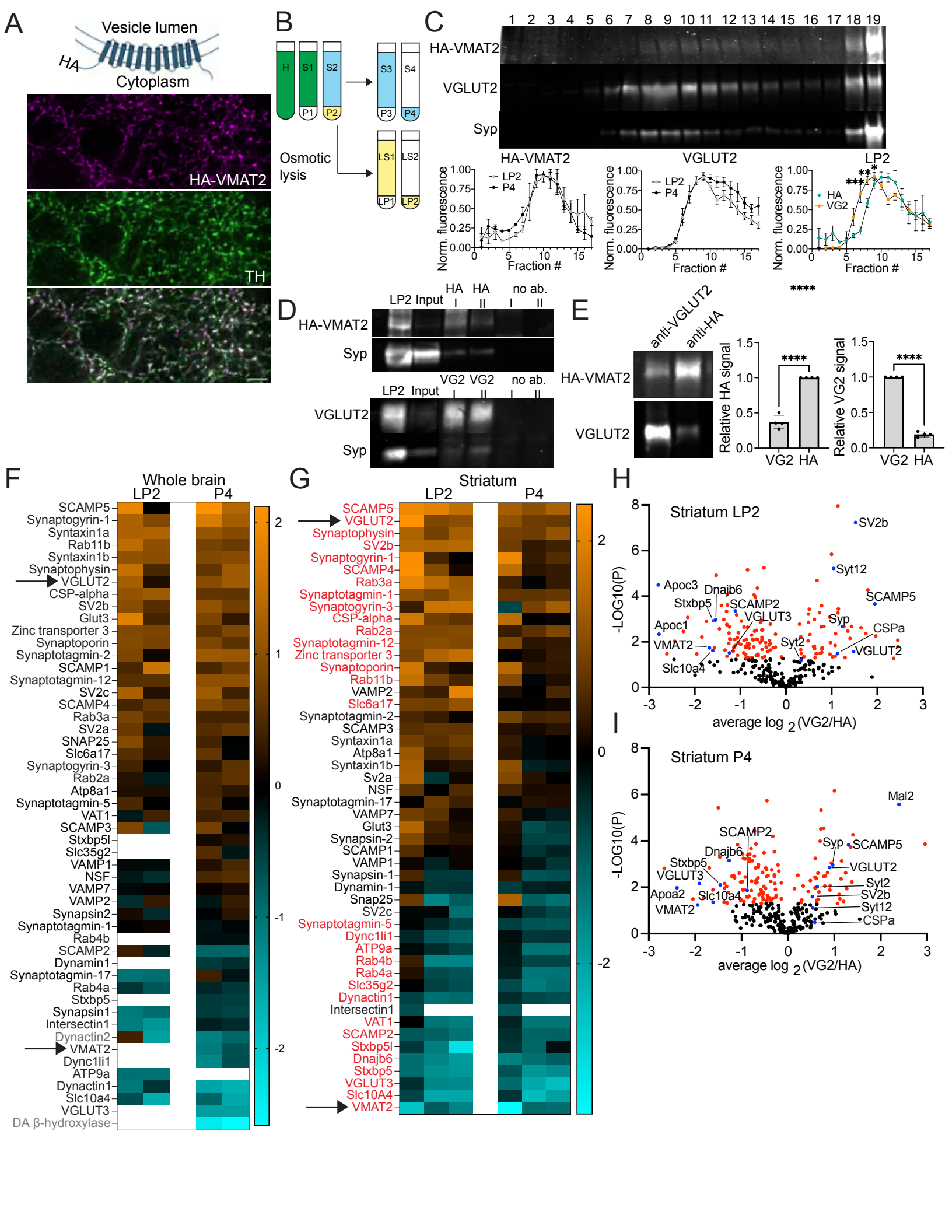
A
Vesicle lumen
HA
Cytoplasm
HA-VMAT2
TH
B
H
S1
S2
S3
S4
P1
P2
P3
P4
Osmotic lysis
LS1
LS2
LP1
LP2
C
1 2 3 4 5 6 7 8 9 10 11 12 13 14 15 16 17 18 19
HA-VMAT2
VGLUT2
Syp
HA-VMAT2
VGLUT2
LP2
LP2
P4
HA
VG2
Norm. fluorescence
Fraction #
D
LP2 Input
HA I
HA II
no ab. I
no ab. II
HA-VMAT2
Syp
VG2 I
VG2 II
VGLUT2
E
anti-VGLUT2
anti-HA
HA-VMAT2
VGLUT2
Relative HA signal
Relative VG2 signal
****
VG2
HA
F
Whole brain
LP2
P4
SCAMP5
Synaptogyrin-1
Syntaxin1a
Rab11b
Syntaxin1b
Synaptophysin
VGLUT2
CSP-alpha
SV2b
Glut3
Zinc transporter 3
Synaptoporin
Synaptotagmin-2
SCAMP1
Synaptotagmin-12
SV2c
SCAMP4
Rab3a
SV2a
SNAP25
Slc6a17
Synaptogyrin-3
Rab2a
Atp8a1
Synaptotagmin-5
VAT1
SCAMP3
Stxbp5l
Slc35g2
VAMP1
NSF
VAMP7
VAMP2
Synapsin2
Synaptotagmin-1
Rab4b
SCAMP2
Dynamin1
Synaptotagmin-17
Rab4a
Stxbp5
Synapsin1
Intersectin1
Dynactin2
VMAT2
Dync1li1
ATP9a
Dynactin1
Slc10a4
VGLUT3
DA β-hydroxylase
G
Striatum
LP2
P4
SCAMP5
VGLUT2
Synaptophysin
SV2b
Synaptogyrin-1
SCAMP4
Rab3a
Synaptotagmin-1
Synaptogyrin-3
CSP-alpha
Rab2a
Synaptotagmin-12
Zinc transporter 3
Synaptoporin
Rab11b
VAMP2
Slc6a17
Synaptotagmin-2
SCAMP3
Syntaxin1a
Atp8a1
Syntaxin1b
Sv2a
NSF
Synaptotagmin-17
VAMP7
Glut3
Synapsin-2
SCAMP1
VAMP1
Synapsin-1
Dynamin-1
Snap25
SV2c
Synaptotagmin-5
Dync1li1
ATP9a
Rab4b
Rab4a
Slc35g2
Dynactin1
Intersectin1
VAT1
SCAMP2
Stxbp5l
Dnajb6
Stxbp5
VGLUT3
Slc10A4
VMAT2
H
Striatum LP2
-LOG10(P)
average log 2 (VG2/HA)
SV2b
Syt12
Apoc3
Dnajb6
Stxbp5
SCAMP2
VGLUT3
SCAMP5
Syp
CSPa
Apoc1
VMAT2
Syt2
VGLUT2
Slc10a4
I
Striatum P4
Mal2
SCAMP2
Syp
SCAMP5
Dnajb6
Stxbp5
VGLUT2
VGLUT3
Syt2
Apoa2
Slc10a4
SV2b
VMAT2
Syt12
CSPa

Figure 1. Isolation and proteomic profiling of VMAT2$^+$ and VGLUT2$^+$ SVs.

A. We used CRISPR to generate a knock-in mouse with an HA tag in the cytoplasmic N-terminus of VMAT2. Confocal image of the striatum stained for HA and TH shows HA-VMAT2 signal in TH-positive axonal fibers. Scale bar = 5 µm.

B. Scheme of the protocol for isolating synaptic vesicles. Synaptosomes from P2 pellet fraction were subjected to osmotic lysis to release synaptic vesicles from presynaptic terminals. Released vesicles (LS1) were separated from synaptic plasma membranes (LP1) and then sedimented in the LP2 pellet. In parallel, we collected light organelles from supernatant S2 to isolate axonal vesicles that were not concentrated in varicosities (P4). Fractions highlighted in color were used in the following steps.

C. Western blot of HA-VMAT2, VGLUT2 and synaptophysin signal in LP2 samples loaded on a 5-25% glycerol gradient. 10 µL of a 500 µL fraction was loaded per lane.

Graphs show the comparison of mean HA-VMAT2 and VGLUT2 signal intensities in gradient fractions of LP2 and P4 samples and the comparison of HA-VMAT2 versus VGLUT2 signal in LP2 samples quantified on dot blots. Data indicate mean ± SEM. * < 0.05, ** < 0.001, *** <0.001, by unpaired t-test

D. Immunoblots showing HA-VMAT2 and synaptophysin (left) or VGLUT2 and synaptophysin (right) in LP2, starting material for vesicle isolation (LP2 after gradient purification and dialysis) and on Dynabeads with antibody used for isolation or in a negative control where antibody was not added.

E. Immunoblots and quantification of HA-VMAT2 and VGLUT2 signal in vesicles immunoisolated using anti-VGLUT2 or anti-HA antibodies. Data indicate mean ± SEM. **** <0.0001, by unpaired t-test

F. Examples of proteins quantified on VMAT2 and VGLUT2 SVs isolated from whole brain samples from HA-VMAT2 KI mice. Data was normalized to the amount of total protein in each sample and is presented as a heat map of log2 values of VGLUT2/VMAT2 ratio. Each column represents an independent experiment. Proteins indicated in gray are not detected in samples from the striatum.

G. Examples of proteins quantified on VMAT2 and VGLUT2 SVs isolated from striatal samples of HA-VMAT2 KI mice. Data was normalized to the amount of total protein in each sample and is presented as a heat map of log2 values of VGLUT2/VMAT2 ratio. Each column represents an independent experiment. Proteins highlighted in red show significant enrichment in one SV population ($P < 0.05$) and have a VGLUT2/VMAT2 ratio above 1.5 or below -1.5.

H-I. Volcano plots showing protein abundance in VMAT2 versus VGLUT2 SVs in striatal LP2 (H) and P4 samples (I) as determined by TMT labeling and mass spectrometry. Data was analyzed in three independent experiments. Data points highlighted in red have p-values < 0.05. Blue data points are associated with labels.

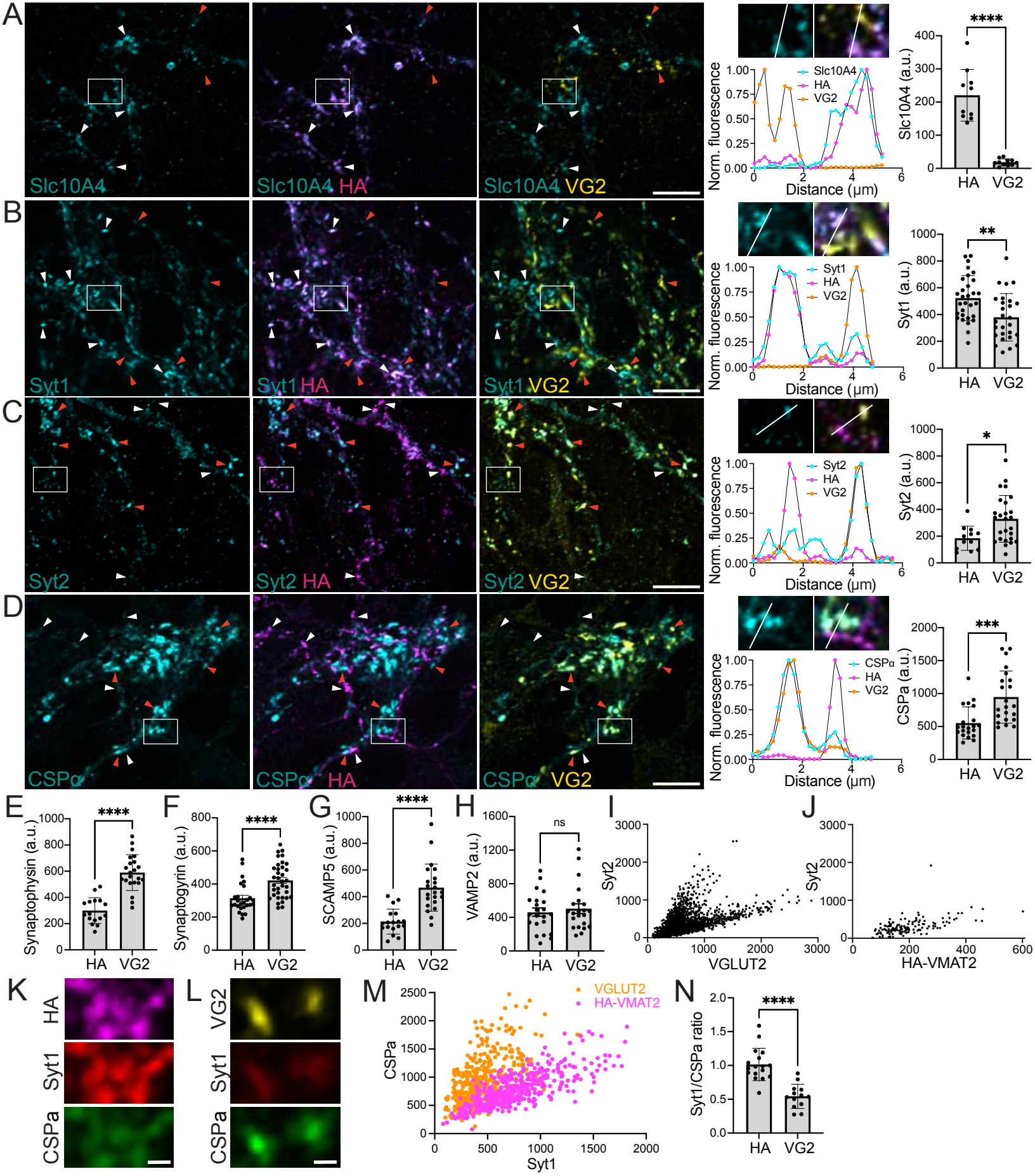
A
Slc10A4
Slc10A4 HA
Slc10A4 VG2
Norm. fluorescence
Distance (μm)
Slc10A4
HA
VG2
Slc10A4 (a.u.)
****
B
Syt1
Syt1 HA
Syt1 VG2
Syt1 (a.u.)
**
C
Syt2
Syt2 HA
Syt2 VG2
Syt2 (a.u.)
*
D
CSPα
CSPα HA
CSPα VG2
CSPa (a.u.)
***
E
Synaptophysin (a.u.)
****
F
Synaptogyrin (a.u.)
****
G
SCAMP5 (a.u.)
****
H
VAMP2 (a.u.)
ns
I
Syt2
VGLUT2
J
Syt2
HA-VMAT2
K
HA
Syt1
CSPa
L
VG2
Syt1
CSPa
M
VGLUT2
HA-VMAT2
CSPa
Syt1
N
Syt1/CSPa ratio
****

Figure 2. Dopamine and glutamate release sites in primary midbrain neurons differ in composition.

A-D. Confocal images of midbrain cultures from HA-VMAT2 KI mice showing the distribution of Slc10A4 (A), syt1 (B), syt2 (C) and CSPα (D) in VMAT2 and VGLUT2 varicosities and the quantification of mean fluorescence intensity of the proteins of interest in the two types of release sites. White arrowheads point to VMAT2 and orange arrowheads to VGLUT2 varicosities. Scale bars = 10 μm. Inset shows magnification of the area indicated by the white box and a line ROI with corresponding fluorescence profiles in three channels shown below.

E-H. Quantification of mean fluorescence intensity of synaptophysin (E), synaptogyrin1 (F), SCAMP5 (G) and VAMP2 (H) in DA release sites identified as HA-VMAT2 clusters in TH+ cells and in VGLUT2-positive glutamate release sites. Each data point represents the mean intensity of the signal for proteins of interest in all ROIs per image.

I-J. Scatter plot of syt2 and VGLUT2 (I) and syt2 and HA-VMAT2 (J) fluorescence intensity in individual release sites.

K-N. Presynaptic varicosities stained for HA-VMAT2, synaptotagmin1 and CSPα (K) or VGLUT2, synaptotagmin1 and CSPα (L). Scale bar = 1 μm. Scatter plot of intensities of CSPα and syt1 signal quantified in individual HA-VMAT2 or VGLUT2 varicosities (M) and quantification of syt1/CSPα ratio averaged per image (N).

Data indicate mean ± SEM in all panels. * < 0.05, ** <0.01, *** < 0.001, **** <0.0001, by unpaired t-test (A, B, C, E, G, N), or Mann-Whitney test (D, F, H).

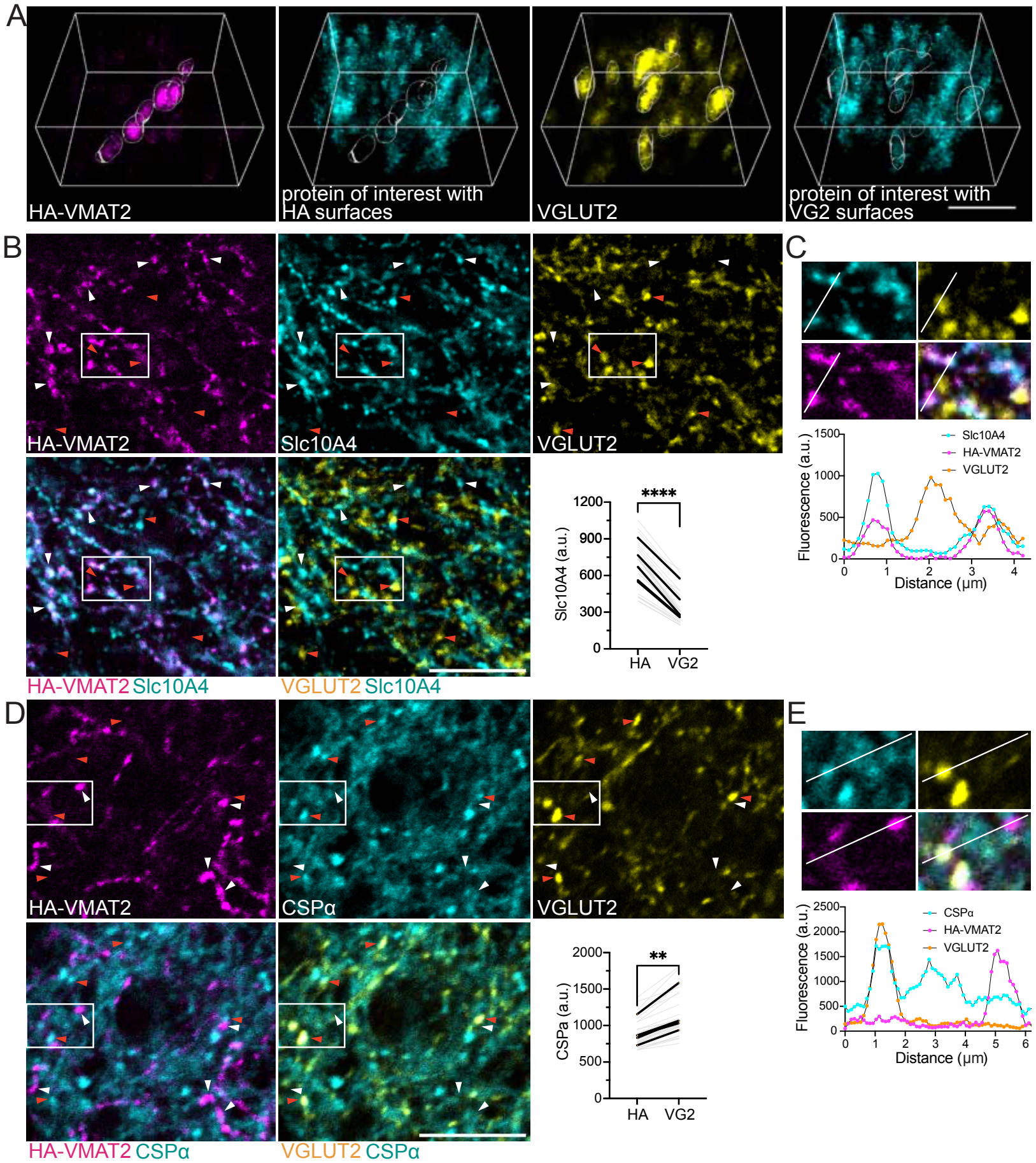
A
HA-VMAT2
protein of interest with HA surfaces
VGLUT2
protein of interest with VG2 surfaces
B
HA-VMAT2
Slc10A4
VGLUT2
HA-VMAT2 Slc10A4
VGLUT2 Slc10A4
****
Slc10A4 (a.u.)
1200
900
600
300
0
HA
VG2
C
Slc10A4
HA-VMAT2
VGLUT2
Fluorescence (a.u.)
1500
1000
500
0
0
1
2
3
4
Distance (µm)
D
HA-VMAT2
CSPα
VGLUT2
HA-VMAT2 CSPα
VGLUT2 CSPα
**
CSPa (a.u.)
2000
1500
1000
500
0
HA
VG2
E
CSPα
HA-VMAT2
VGLUT2
Fluorescence (a.u.)
2500
2000
1500
1000
500
0
0
1
2
3
4
5
6
Distance (µm)

Figure 3. Dopamine release sites and VGLUT2^{+} glutamate terminals in the striatum differ in the abundance of SV proteins.

A. Example of 3D surfaces generated in a striatal z-stack of a staining for HA-VMAT2 (magenta) or VGLUT2 (yellow). The same surfaces are transferred to the channel showing the staining for a protein of interest (cyan) for quantification of its the mean intensity in HA-VMAT2 and VGLUT2 surfaces. Scale bar = 4 µm.

B-C. B. Confocal image of a single plane in a striatal slice from a HA-VMAT2 KI mouse stained for HA-VMAT2, Slc10A4 and VGLUT2 together with quantification of mean Slc10A4 intensity in 3D surfaces generated based on HA-VMAT2 or VGLUT2 signal. Gray lines show mean values of varicosities per image, black lines indicate the mean values per mouse. **** <0.0001 by paired t-test on mouse averages. Scale bar = 10 µm. White arrowheads point to HA-VMAT2 and orange arrowheads to a VGLUT2 varicosities. C. Magnified view of the area highlighted by white box in B and plot profile of fluorescence intensities in three channels along the line ROI.

D-E. D. Confocal image of a single plane in a striatal slice from a HA-VMAT2 KI mouse stained for HA-VMAT2, CSPα and VGLUT2 together with quantification of mean CSPα intensity in 3D surfaces generated based on HA-VMAT2 or VGLUT2 signal. Gray lines show mean values of varicosities per image, black lines indicate the mean values per mouse. ** = 0.006 by paired t-test on mouse averages. Scale bar = 10 µm. White arrowheads point to HA-VMAT2 and orange arrowheads to a VGLUT2 varicosities. Magnified view of the area highlighted by white box in D and plot profile of fluorescence intensities in three channels along the line ROI.

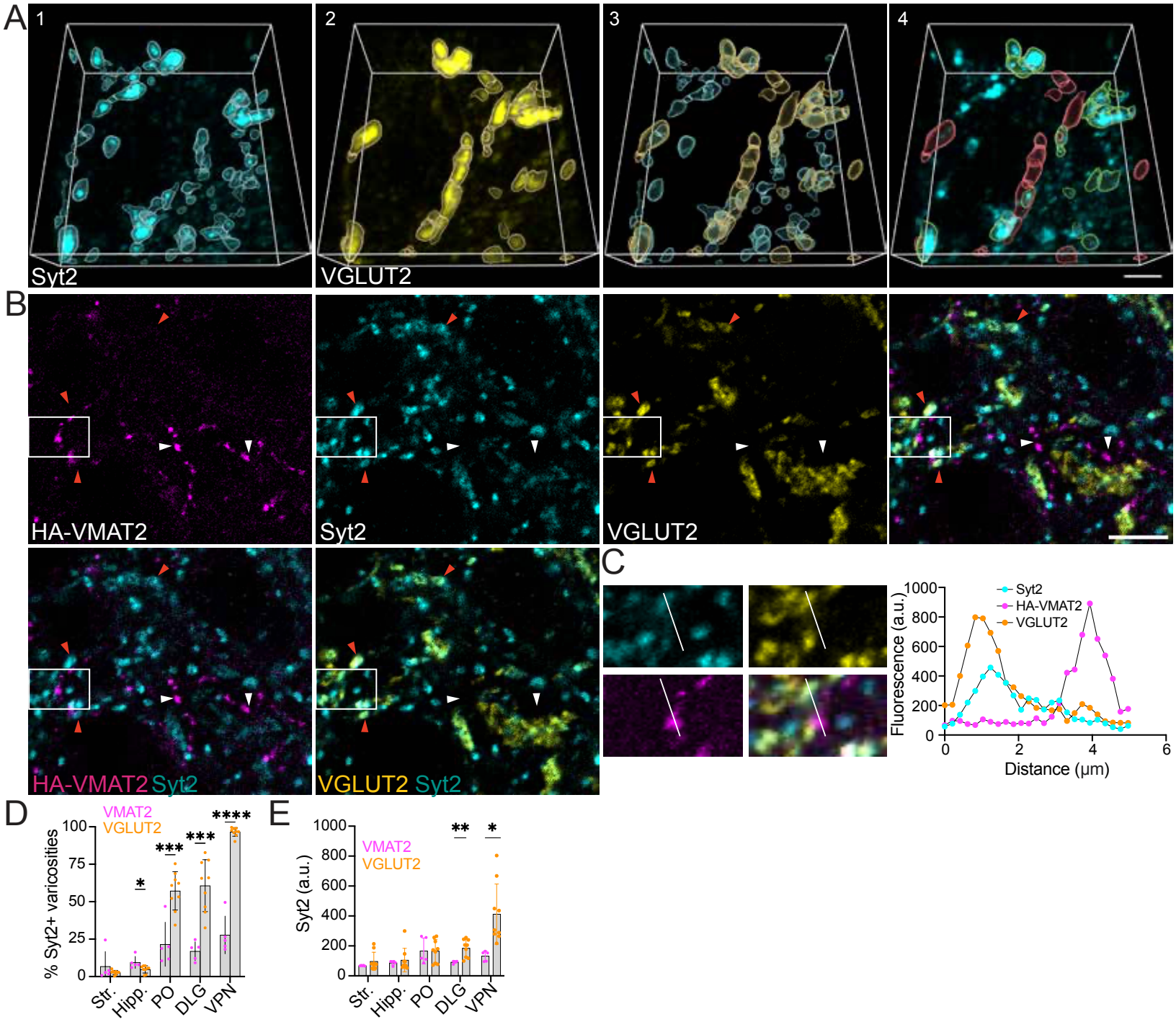

Figure 4. Expression of syt2 reveals heterogeneity among VGLUT2+ glutamate neurons.

A. Example of 3D surfaces generated in a z-stack based on staining for syt2 (cyan, panel 1) or VGLUT2 (yellow, panel 2). Panel 3 shows syt2 and VGLUT2 surfaces in the same 3D section. In panel 4, syt2-positive VGLUT2 surfaces are shown in green and syt2-negative VGLUT2 surfaces are shown in red. A varicosity is considered syt2-positive if >40% of its volume overlaps with syt2 signal. Scale bar = 4 µm.

B. A single plane of a confocal image of a fixed brain slice from a HA-VMAT2 KI mouse acquired in the lateral geniculate nucleus (DLG). The slice is stained for HA-VMAT2, syt2 and VGLUT2. White arrowheads point to VMAT2 and orange arrowheads to a VGLUT2 varicosities. Scale bar = 3 µm.

C. Magnified view of the area highlighted by white box in B and plot profile of fluorescence intensities in three channels along the line ROI.

D. Percentage of VGLUT2 and HA-VMAT2 varicosities that contain syt2 signal in different brain regions. Each data point represents the percentage of syt2-positive varicosities per z-stack. Data indicate mean ± SEM. * = 0.0175, *** < 0.001, **** < 0.0001 by two-tailed unpaired t-test.

E. Quantification of mean syt2 intensity in HA-VMAT2 and VGLUT2 surfaces across brain regions. Each data point represents an analyzed z-stack. Data indicate mean ± SEM. * = 0.0105, ** = 0.0047 by two-tailed unpaired t-test.

Str. – striatum, Hipp. – CA2 region of the hippocampus, PO – posterior complex, VPN – ventral posteromedial nucleus.

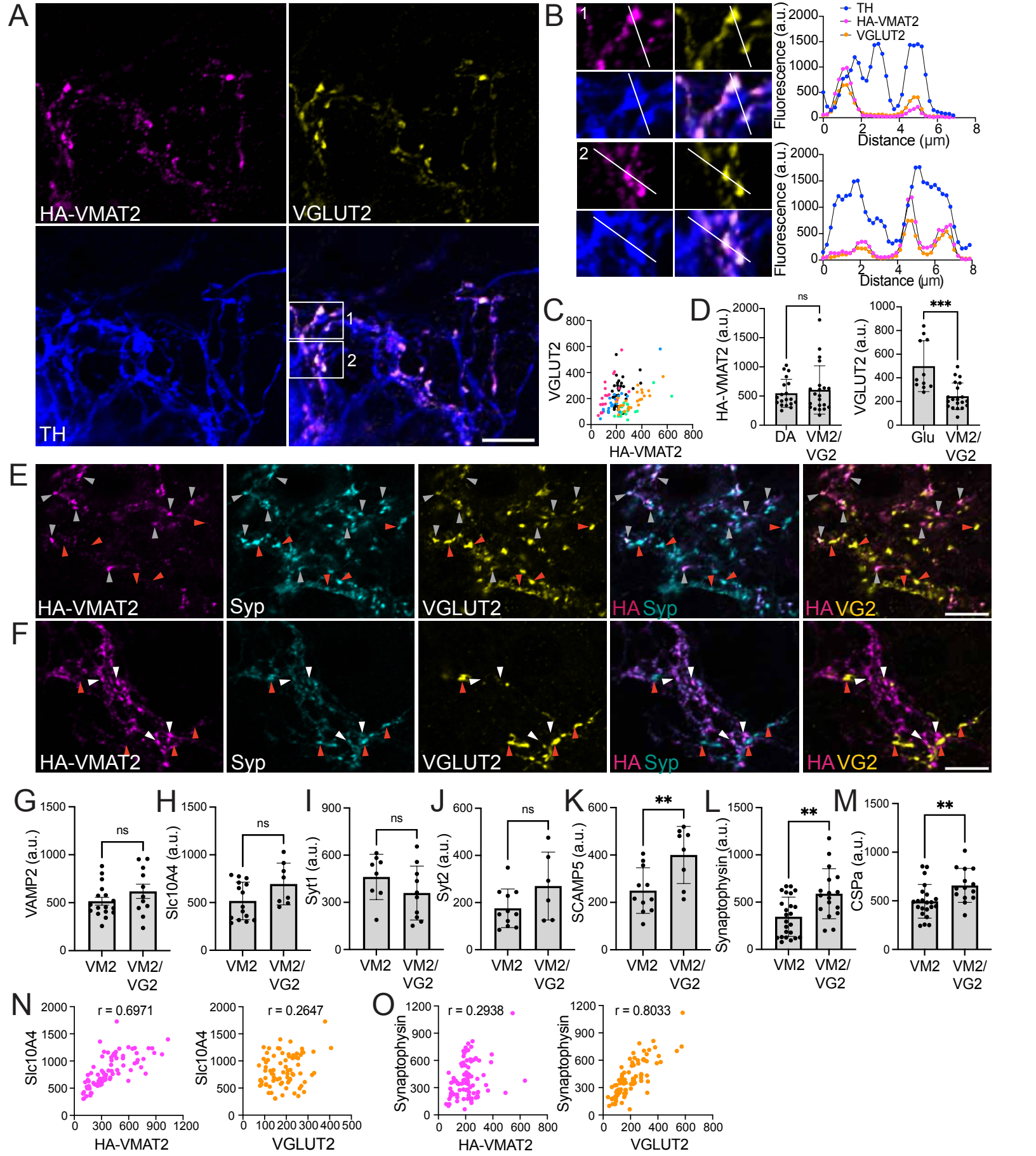
A
HA-VMAT2
VGLUT2
TH
1
2
B
TH
HA-VMAT2
VGLUT2
Fluorescence (a.u.)
Distance (μm)
C
VGLUT2
HA-VMAT2
D
HA-VMAT2 (a.u.)
ns
DA
VM2/VG2
VGLUT2 (a.u.)
***
Glu
E
HA-VMAT2
Syp
VGLUT2
HA Syp
HA VG2
F
G
VAMP2 (a.u.)
H
Slc10A4 (a.u.)
I
Syt1 (a.u.)
J
Syt2 (a.u.)
K
SCAMP5 (a.u.)
**
L
Synaptophysin (a.u.)
M
CSPa (a.u.)
VM2
VM2/VG2
N
r = 0.6971
Slc10A4
HA-VMAT2
r = 0.2647
VGLUT2
O
r = 0.2938
Synaptophysin
r = 0.8033

Figure 5. SV protein composition of VMAT2-only versus VMAT2$^+$/VGLUT2$^+$ release sites.

A. Confocal image of a VGLUT2-positive DA neuron in a primary midbrain culture from HA-VMAT2 KI mice. Scale bar = 10 µm.

B. Magnified view of areas indicated by white boxes in A and plot profile of HA-VMAT2, VGLUT2 and TH signal along the line ROI showing overlapping VGLUT2 and HA-VMAT2 peaks in a DA neuron.

C. Scatter plot of HA-VMAT2 and VGLUT2 signal in individual presynaptic varicosities from one data set. Each color represents varicosities from one image (likely corresponding to a single cell).

D. Quantification of HA-VMAT2 signal in the presynaptic terminals of dopamine-only versus VMAT2$^+$/VGLUT2$^+$ neurons and VGLUT2 signal in glutamate-only versus VMAT2$^+$/VGLUT2$^+$ neurons. Each data point represents mean of individual ROIs per image. Data indicate mean ± SEM. *** = 0.0006 by Mann-Whitney test.

E. Confocal image of a coreleasing neuron and adjacent glutamate-only terminals stained for TH (not shown), synaptophysin, HA-VMAT2 and VGLUT2. Gray arrowheads point to VGLUT2$^+$/VMAT2$^+$ varicosities and orange arrowheads to VGLUT2-only terminals. Note that all HA-VMAT2 varicosities have detectable VGLUT2 signal. Scale bar = 10 µm.

F. Confocal image of a dopamine-only neuron and an adjacent glutamate-only neuron stained for TH (not shown), synaptophysin, HA-VMAT2 and VGLUT2. White arrowheads point to VMAT2 terminals and orange arrowheads to VGLUT2 terminals. Scale bar = 10 µm.

G-M. Quantification of VAMP2 (G), Slc10A4 (H), syt1 (I), syt2 (J), SCAMP5 (K), synaptophysin (L) and CSPα (M) in presynaptic terminals of dopamine-only or VMAT2$^+$/VGLUT2$^+$ neurons. Data indicate mean ± SEM. Each data point represents mean intensity of the signal for a protein of interest in all presynaptic varicosities per image. Data indicate mean ± SEM. ** <0.01 by unpaired t-test (K, M) or Mann-Whitney test (L).

N. Scatterplots showing correlation between Slc10A4 and HA-VMAT2 (magenta) or Slc10A4 and VGLUT2 (orange) signal in the same set of presynaptic terminals that contain both VGLUT2 and VMAT2.

O. Scatterplots showing correlation between synaptophysin and HA-VMAT2 (magenta) or synaptophysin and VGLUT2 (orange) signal in the same set of presynaptic terminals that contain both VGLUT2 and VMAT2.

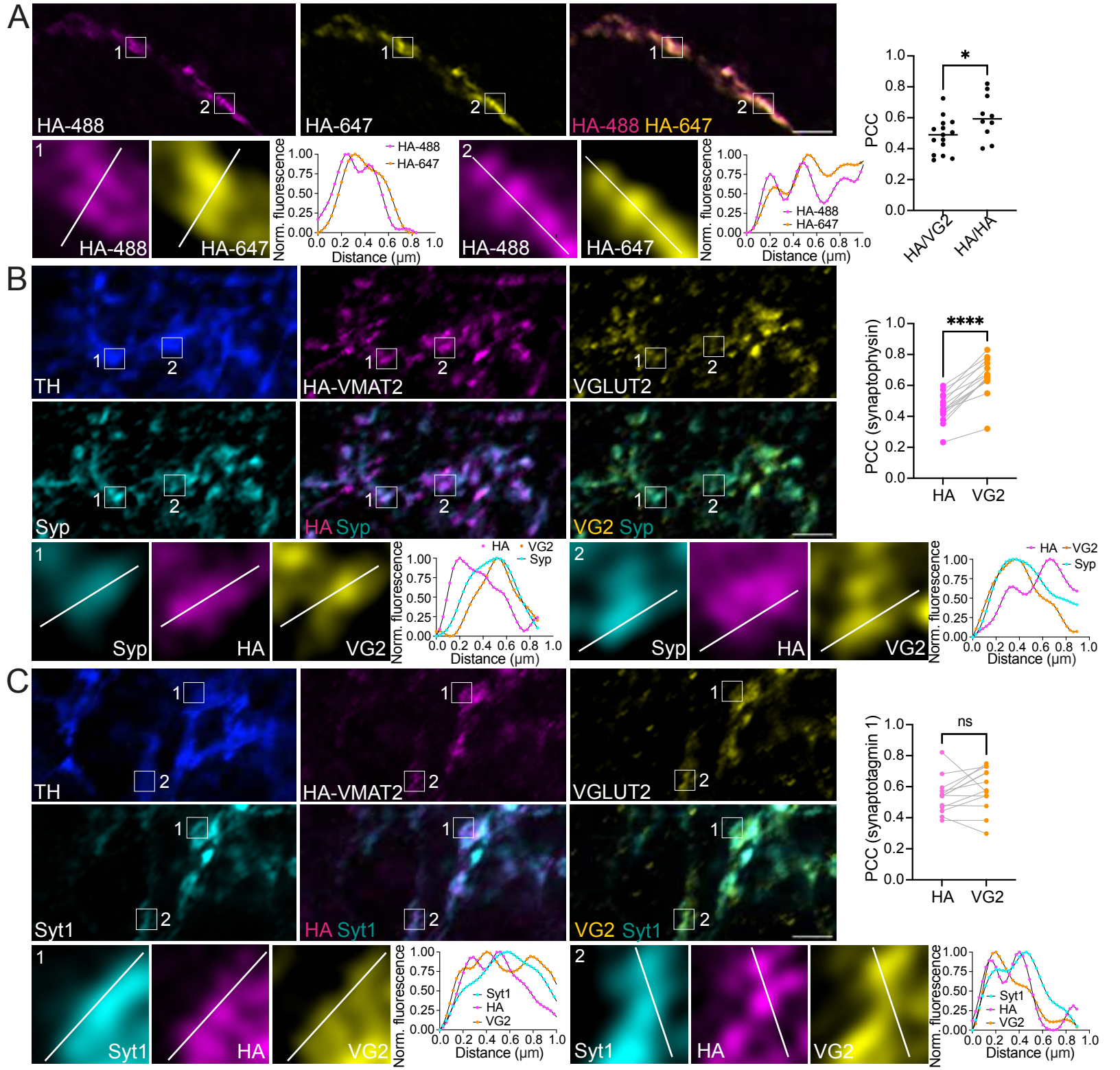
A
HA-488
HA-647
HA-488 HA-647
Norm. fluorescence
Distance (µm)
PCC
HA/VG2
HA/HA
B
TH
HA-VMAT2
VGLUT2
Syp
HA Syp
VG2 Syp
PCC (synaptophysin)
HA
VG2
C
Syt1
HA Syt1
VG2 Syt1
PCC (synaptotagmin 1)
ns

Figure 6. Synaptophysin is co-enriched with VGLUT2 in dopamine neuron presynaptic varicosities that contain both VMAT2 and VGLUT2.

A. Dopamine neuron from an HA-VMAT2 culture double stained for HA-VMAT2 using secondary antibodies coupled with Alexa 488 and Alexa 647 fluorophores. Scale bar = 2 µm.

Quantification shows Pearson's correlation coefficient (PCC) in individual varicosities for HA imaged in two channels versus for HA and VGLUT2 measured in data sets shown in B and C. Data indicate mean ± SEM. Each data point represents the mean of individual varicosities per image. * = 0.0265 by unpaired t-test. N = 10 HA/HA and 15 HA/VGLUT2 coverslips from two independent cultures.

Insets show magnification of areas indicated with white boxes with line ROIs and fluorescence profiles in HA-488 and HA-647 channels.

B. VGLUT2$^+$ DA neuron from an HA-VMAT2 midbrain culture stained for TH, HA, VGLUT2 and synaptophysin (syp). Scale bar = 2 µm.

Quantification shows Pearson's correlation coefficient (PCC) for HA and synaptophysin versus VGLUT2 and synaptophysin quantified in varicosities that contain all three proteins. Data indicate mean ± SEM. Each data point represents the mean of individual varicosities per image. **** < 0.0001 by paired t-test. N = 14 images from two independent cultures.

Insets show magnification of areas indicated with white boxes with line ROIs and fluorescence profiles in HA, VGLUT2 and synaptophysin channels.

C. VGLUT2$^+$ DA neuron from an HA-VMAT2 midbrain culture stained for TH, HA, VGLUT2 and synaptotagmin1 (syt1). Scale bar = 2 µm.

Quantification shows Pearson's correlation coefficient (PCC) for HA and synaptotagmin1 versus VGLUT2 and synaptotagmin1 quantified in varicosities that contain all three proteins. Data indicate mean ± SEM. Each data point represents the mean of individual varicosities per image. P = 0.2181 by paired t-test. N = 13 images from two independent cultures.

Insets show magnification of areas indicated with white boxes with line ROIs and fluorescence profiles in HA, VGLUT2 and synaptotagmin1 channels.

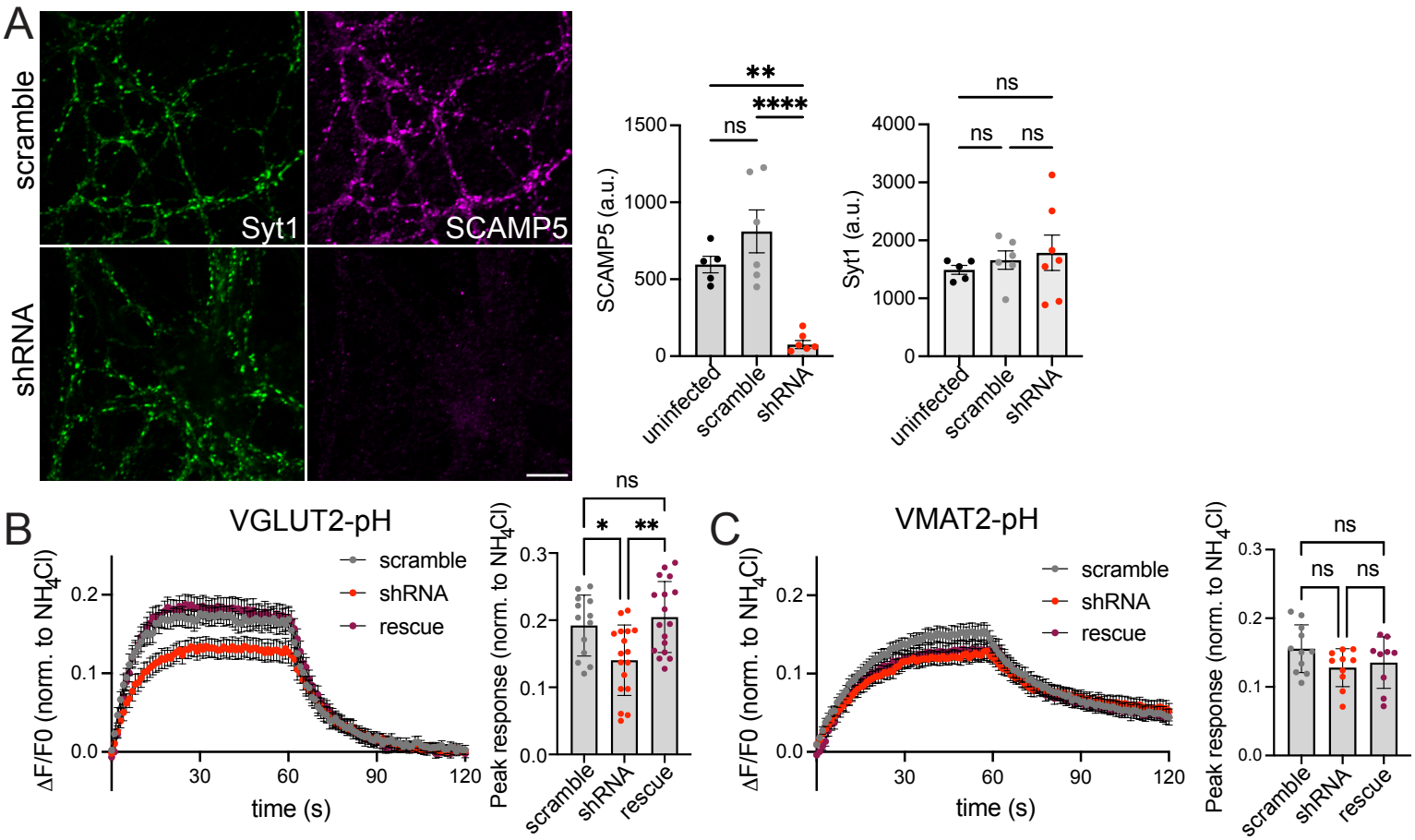

Figure 7. Loss of SCAMP5 impairs synaptic recycling of VGLUT2 SVs without affecting VMAT2.

A. Confocal images and quantification of the fluorescence intensity of synaptotagmin1 and SCAMP5 in uninfected hippocampal neurons or cultures infected with shRNA targeting SCAMP5 or a scrambled control. Each data point represents mean presynaptic SCAMP5 or syt1 intensity per image. Data indicate mean ± SEM, ** $p = 0.0021$, **** $p < 0.0001$ by one-way ANOVA with Tukey's multiple comparisons. n = 5 uninfected, 6 scramble and 7 shRNA coverslips.

B-C. Average response curves and quantification of peak fluorescence intensity of VGLUT2-pHluorin (B) or VMAT2-pHluorin (C) to a 60s stimulation at 10 Hz. Data indicate mean ± SEM, * = 0.0225, ** = 0.017 by one-way ANOVA with Tukey's multiple comparisons.
N = 13 scramble, 17 shRNA and 17 rescue coverslips for VGLUT2-pHluorin and 11 scramble, 10 shRNA and 9 rescue coverslips for VMAT2-pHluorin from three independent cultures.

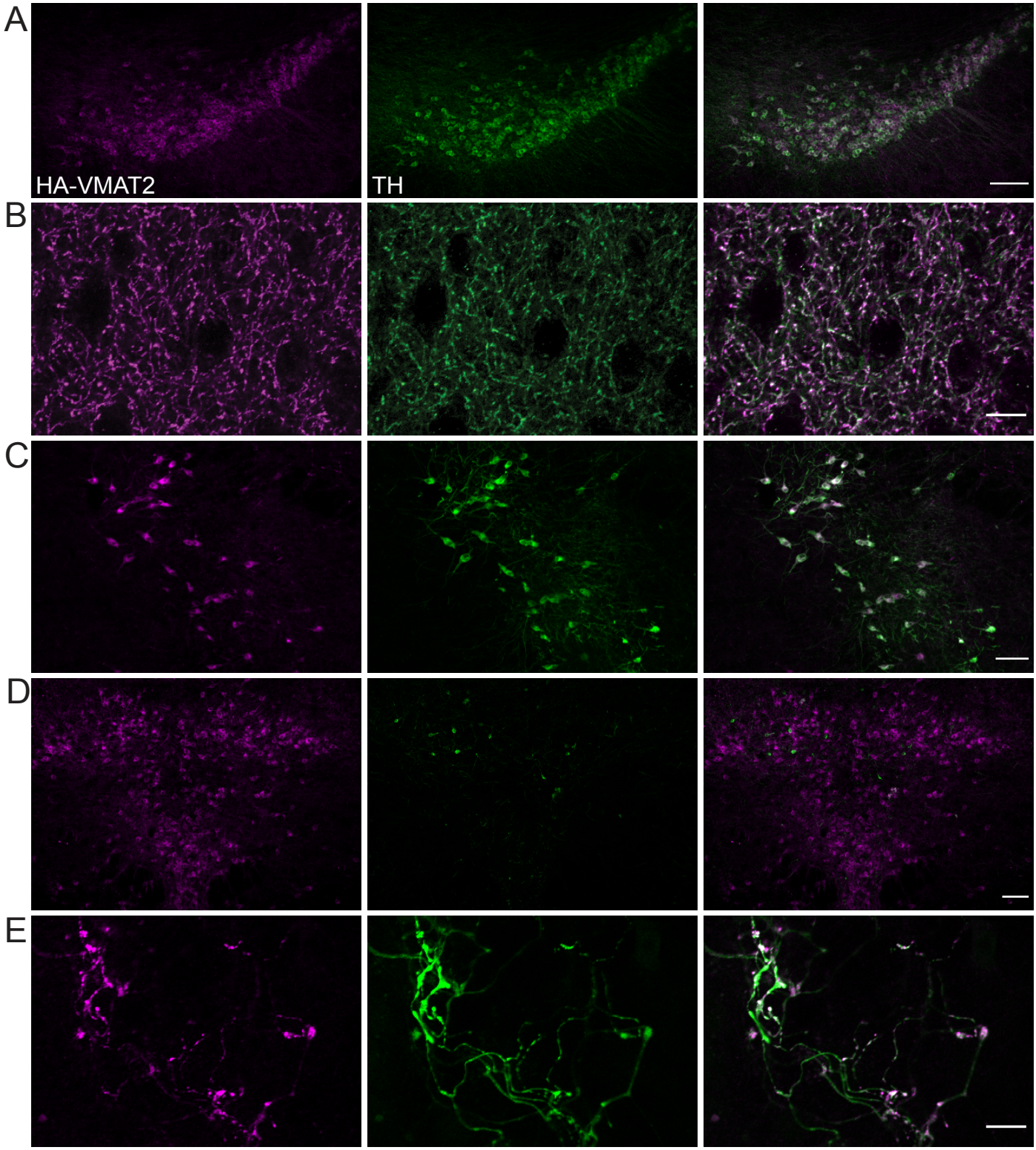

Supplementary figure 1. HA-VMAT2 is localized in cell bodies and neuronal processes of monoamine neurons.

A-D. Representative confocal images of HA-VMAT2 KI brain slices from the midbrain (A), striatum (B), locus coeruleus (C) and the raphe nucleus (D) stained for HA (magenta) and tyrosine hydroxylase (TH, green). Scale bar = 10 μm in all images.

E. Representative confocal image of a midbrain culture form HA-VMAT2 mice. Cultured neuron is stained for HA and TH. Scale bar = 10 μm.

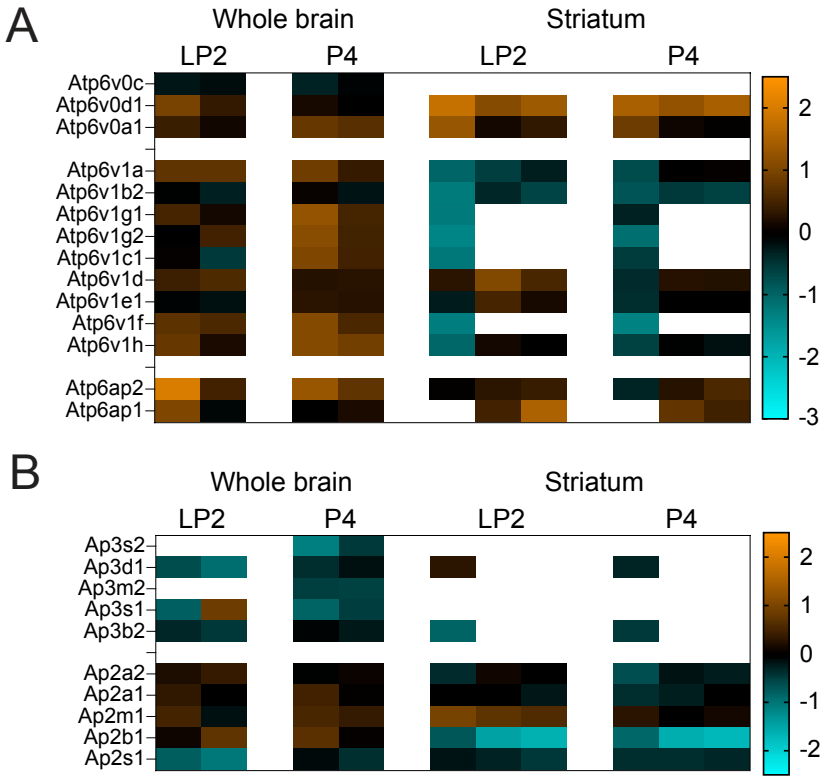

Supplementary figure 2. Abundance of V-ATPase, AP-2 and AP-3 subunits in VMAT2+ and VGLUT2+ SVs.

A. Subunits of the v-ATPase quantified on VMAT2 and VGLUT2 SVs isolated from whole brain or striatal samples from the HA-VMAT2 KI mouse. Data was normalized to the amount of total protein in each sample and is presented as a heat map of log2 values of VGLUT2/VMAT2 ratio. Each column represents an independent experiment.

B. Subunits of AP-2 and AP-3 quantified on VMAT2 and VGLUT2 SVs isolated from whole brain or striatal samples from the HA-VMAT2 KI mouse. Data was normalized to the amount of total protein in each sample and is presented as a heat map of log2 values of VGLUT2/VMAT2 ratio. Each column represents an independent experiment.

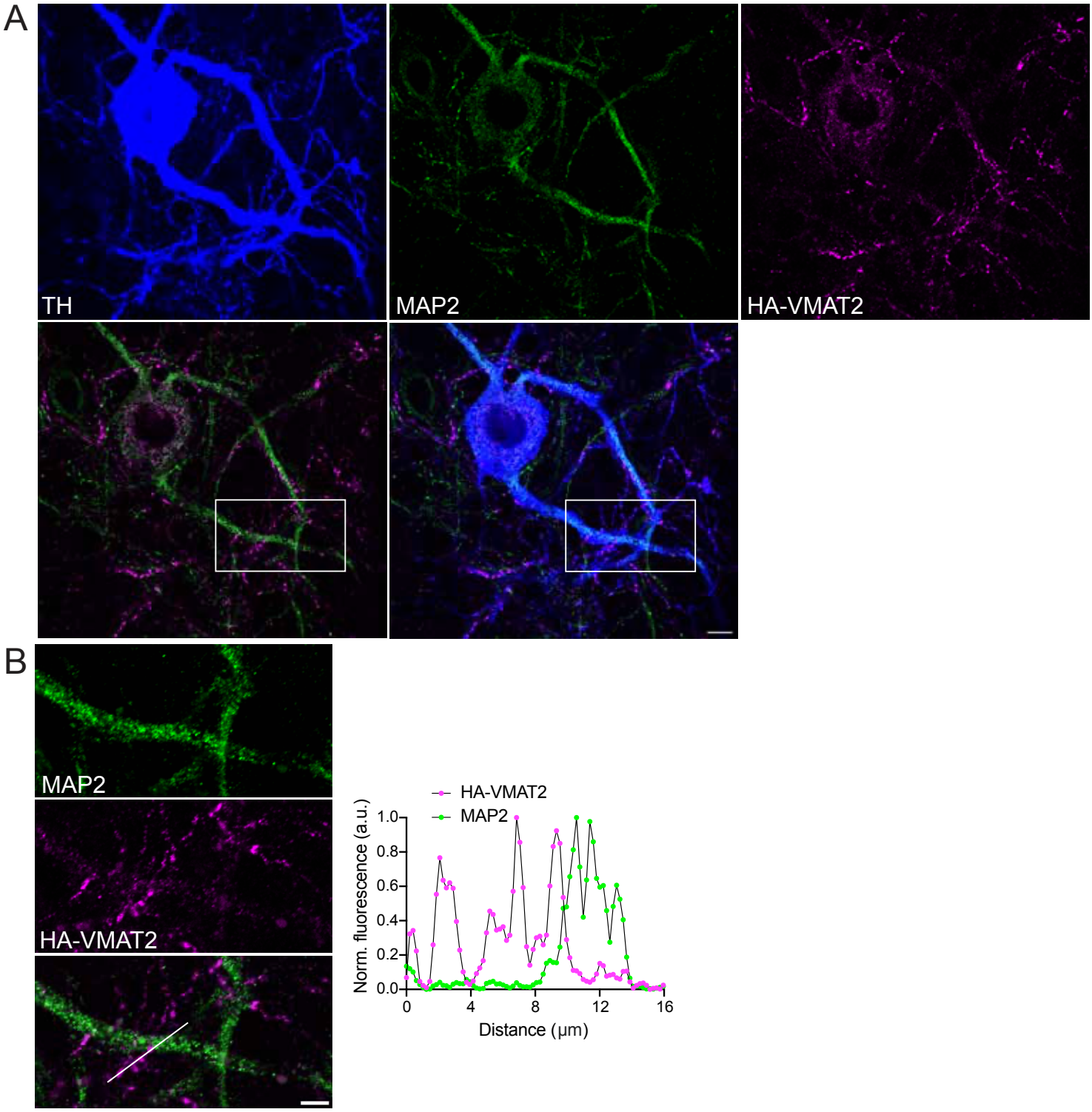

Supplementary figure 3. HA-VMAT2 varicosities represent axonal vesicle clusters.

A. Confocal image of a dopamine neuron in a HA-VMAT2 KI midbrain culture stained for TH, somatodendritic protein MAP2 and HA-VMAT2. Scale bar = 10 µm.

B. Magnified view of the area highlighted by white box in A. Scale bar = 5 µm. Graph shows normalized fluorescence profiles of HA-VMAT2 and MAP2 along the line ROI shown in the merged image.

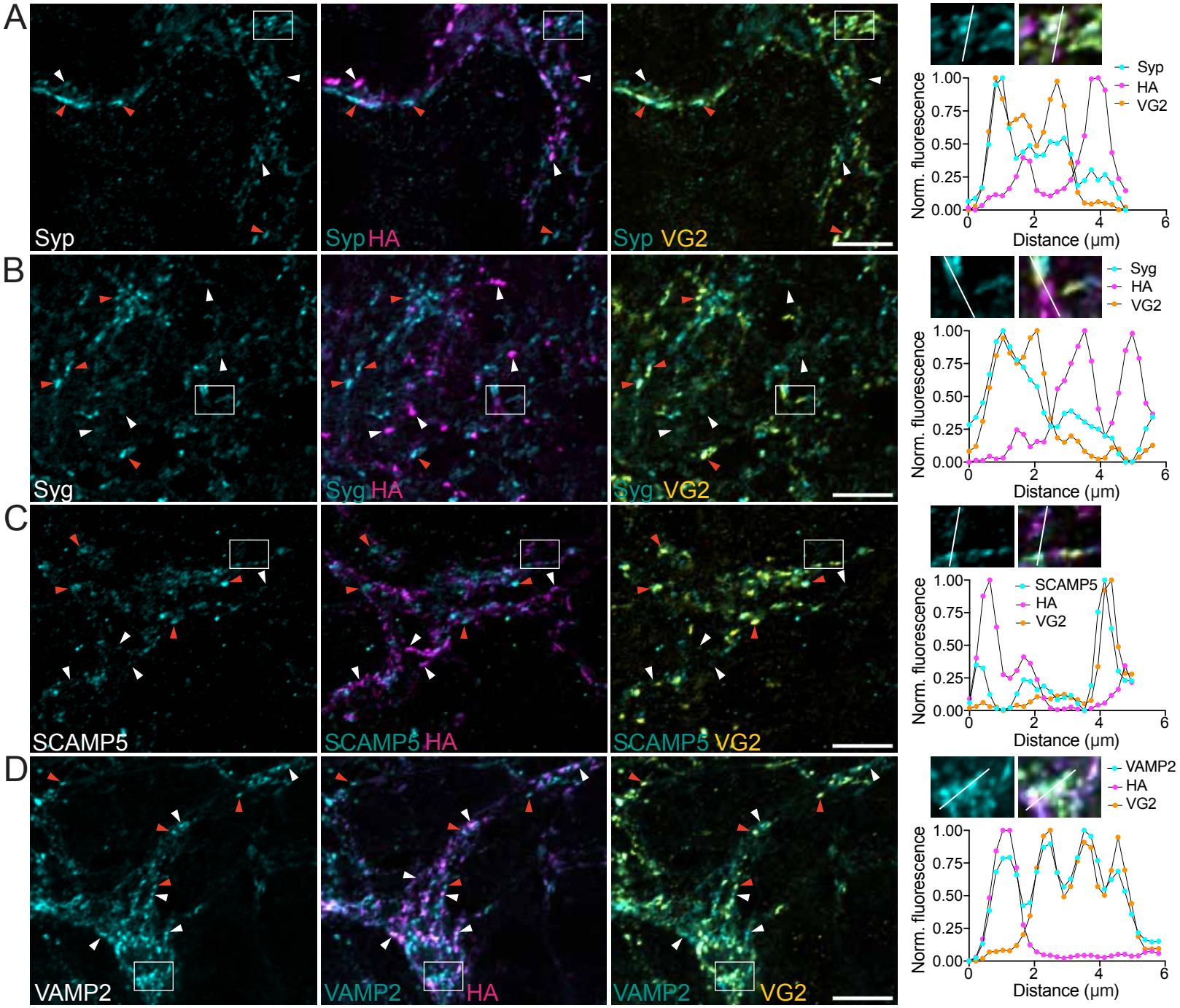

Supplementary figure 4. Presynaptic composition of dopamine and glutamate release sites in primary midbrain cultures.

A-D. Confocal images of midbrain cultures from HA-VMAT2 KI mice stained for HA-VMAT2, VGLUT2 and synaptophysin (A), synaptogyrin1 (B), SCAMP5 (C) or VAMP2 (D). White arrowheads point to HA-VMAT2 and orange arrowheads to VGLUT2 varicosities. Scale bars = 10 µm in all images. Insets show magnification of the area indicated by the white boxes in larger images and a line ROI with corresponding fluorescence profiles in three channels shown below.

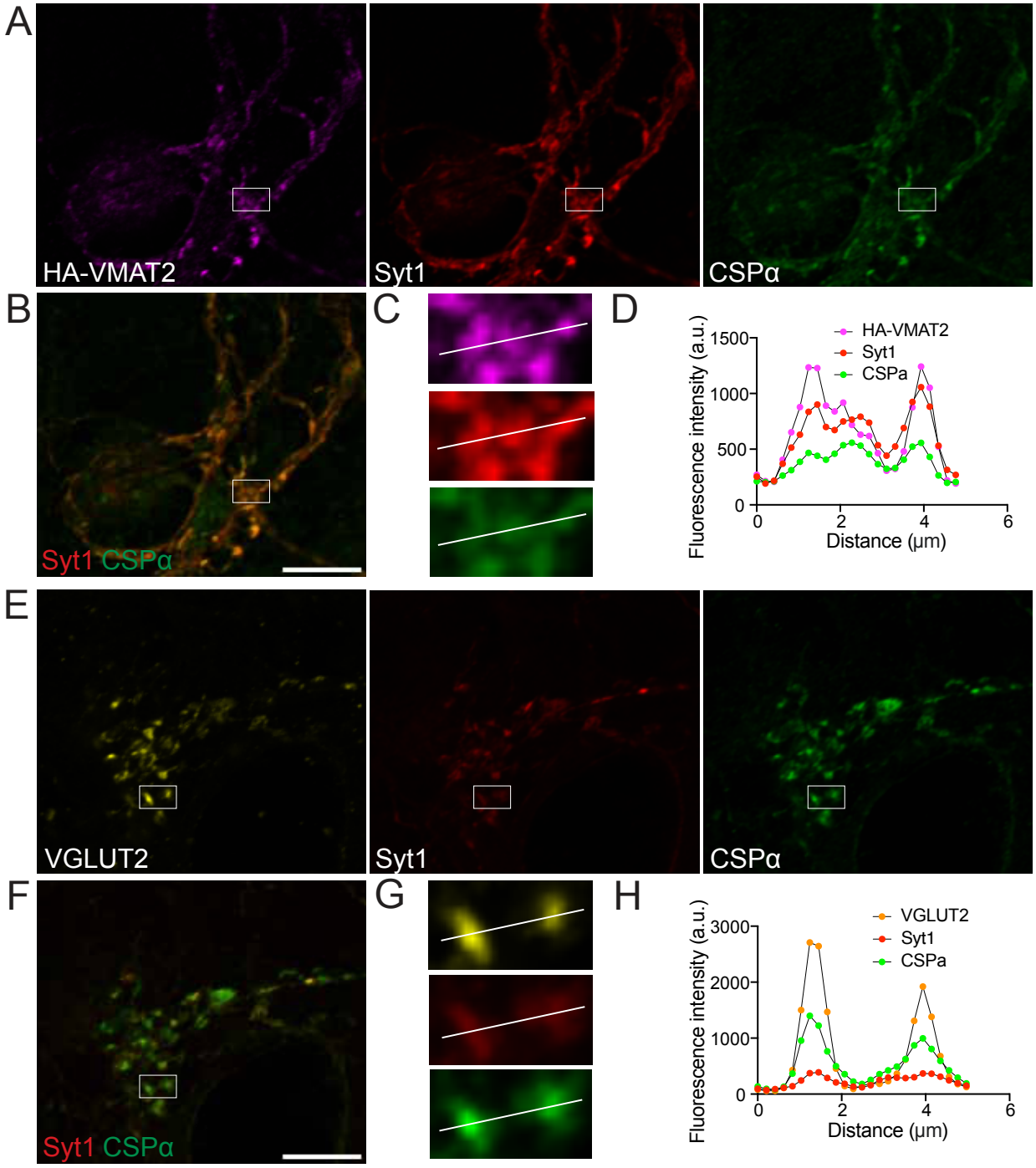

Supplementary figure 5. VMAT2 and VGLUT2 varicosities differ in syt1/CSPα ratio.

A-D. A. Confocal image of a midbrain culture from HA-VMAT2 KI mice stained for HA-VMAT2, synaptotagmin1 and CSPα.
B. Merge of synaptotagmin1 and CSPα channels. Scale bar = 10 μm. C. Magnified view of the area indicated by white box in A and B.
D. Fluorescence profiles of HA-VMAT2, synaptotagmin1 and CSPα along the line ROI shown in C.

E-H. E. Confocal image of a midbrain culture from HA-VMAT2 KI mice stained for VGLUT2, synaptotagmin1 and CSPα. F. Merge of synaptotagmin1 and CSPα channels. Scale bar = 10 μm. G. Magnified view of the area indicated by white box in E and F.
H. Fluorescence profiles of VGLUT2, synaptotagmin1 and CSPα along the line ROI shown in G.

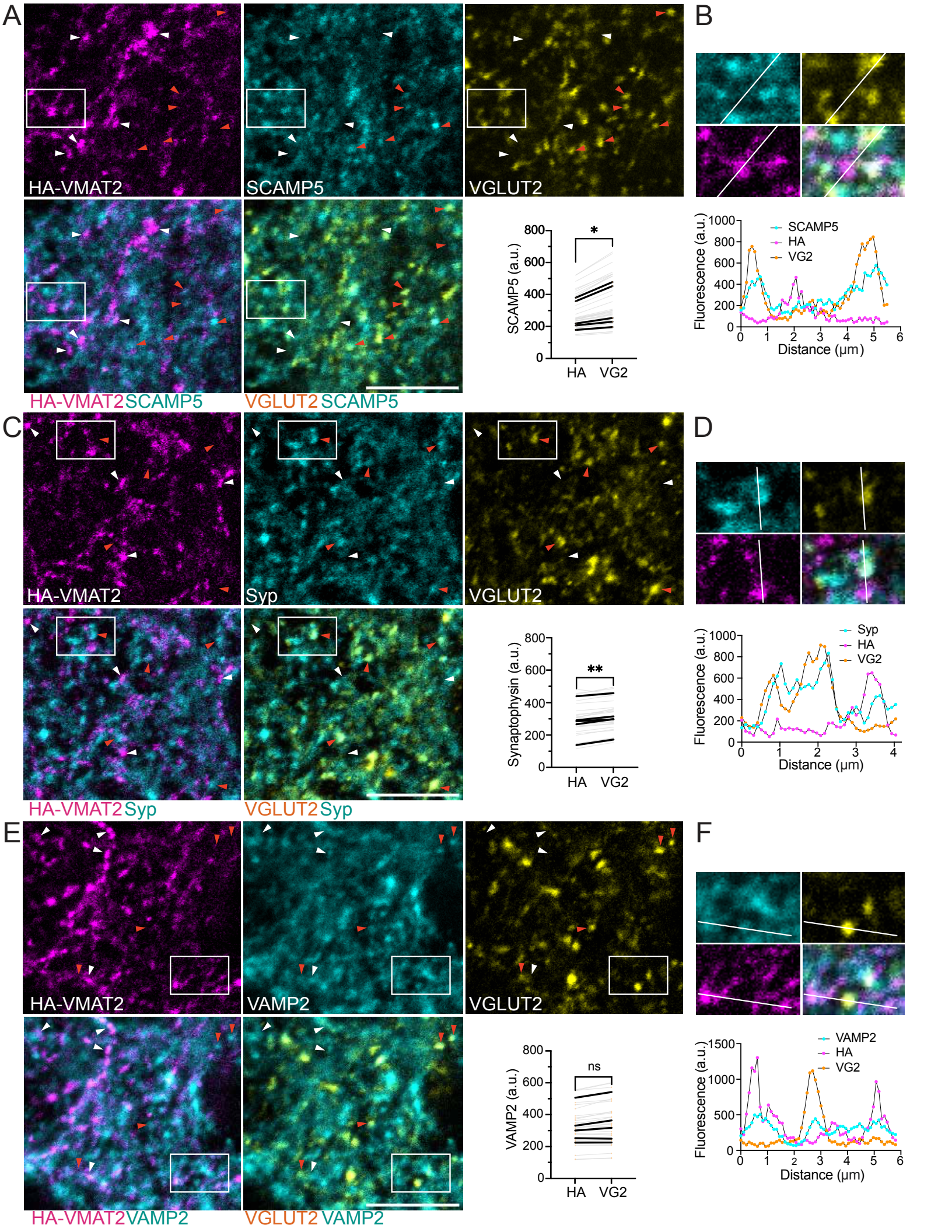
A
HA-VMAT2
SCAMP5
VGLUT2
HA-VMAT2 SCAMP5
VGLUT2 SCAMP5
SCAMP5 (a.u.)
800
600
400
200
0
*
HA
VG2
B
Fluorescence (a.u.)
1000
800
600
400
200
0
SCAMP5
HA
VG2
0 1 2 3 4 5 6
Distance (µm)
C
HA-VMAT2
Syp
VGLUT2
HA-VMAT2 Syp
VGLUT2 Syp
Synaptophysin (a.u.)
800
600
400
200
0
**
HA
VG2
D
Fluorescence (a.u.)
1000
800
600
400
200
0
Syp
HA
VG2
0 1 2 3 4
Distance (µm)
E
HA-VMAT2
VAMP2
VGLUT2
HA-VMAT2 VAMP2
VGLUT2 VAMP2
VAMP2 (a.u.)
800
600
400
200
0
ns
HA
VG2
F
Fluorescence (a.u.)
1500
1000
500
0
VAMP2
HA
VG2
0 1 2 3 4 5 6
Distance (µm)

Supplementary figure 6. Protein composition of VMAT2 and VGLUT2 varicosities in the striatum.

A-B. A. Confocal image of a single plane in a striatal slice from a HA-VMAT2 KI mouse stained for HA-VMAT2, SCAMP5 and VGLUT2 together with quantification of mean SCAMP5 intensity in 3D surfaces generated based on HA-VMAT2 or VGLUT2 signal. Gray lines show mean values of varicosities per image, black lines indicate the mean values per mouse. * = 0.0378 by paired t-test on mouse averages. Scale bar = 10 µm. White arrowheads point to HA-VMAT2 and orange arrowheads to a VGLUT2 varicosities. B. Magnified view of the area highlighted by white box in A and plot profile of fluorescence intensities in three channels along the line ROI.

C-D. C. Confocal image of a single plane in a striatal slice from a HA-VMAT2 KI mouse stained for HA-VMAT2, synaptophysin and VGLUT2 together with quantification of mean synaptophysin intensity in 3D surfaces generated based on HA-VMAT2 or VGLUT2 signal. Gray lines show mean values of varicosities per image, black lines indicate the mean values per mouse. ** = 0.0043 by paired t-test on mouse averages. Scale bar = 10 µm. White arrowheads point to HA-VMAT2 and orange arrowheads to a VGLUT2 varicosities. D. Magnified view of the area highlighted by white box in C and plot profile of fluorescence intensities in three channels along the line ROI.

E-F. E. Confocal image of a single plane in a striatal slice from a HA-VMAT2 KI mouse stained for HA-VMAT2, VAMP2 and VGLUT2 together with quantification of mean VAMP2 intensity in 3D surfaces generated based on HA-VMAT2 or VGLUT2 signal. Gray lines show mean values of varicosities per image, black lines indicate the mean values per mouse. P = 0.1129 by paired t-test on mouse averages. Scale bar = 10 µm. White arrowheads point to HA-VMAT2 and orange arrowheads to a VGLUT2 varicosities. F. Magnified view of the area highlighted by white box in E and plot profile of fluorescence intensities in three channels along the line ROI.

437 **METHODS**

438 **Mice**

439 Both male and female mice were used for all experiments. All mice were housed in group housing,
440 received unlimited food and water and were exposed to 12h/12h light/dark cycle. HA-VMAT2 KI
441 transgenic mice were used for proteomics, primary dopamine neuron cultures and tissue staining.
442 C57BL6J mice were used for primary hippocampal cultures. All experiments with animals were
443 performed according to the National Institutes of Health Guide for Care and Use of Laboratory
444 Animals and were approved by the Cedars-Sinai Medical Center Institutional Animal Care and
445 Use Committee.

446

447 **Generation of HA-VMAT2 knock-in mice**

448 To generate the HA-VMAT2 knock-in mouse model, we used the CRISPR/Cas9 genome editing
449 system. A guide RNA was designed to target the N-terminal tail of mouse VMAT2 (target
450 sequence 5'-CAGCAGCACCAGATCGCTCA-3'). An ssDNA donor template was constructed to
451 contain the sequence of the hemagglutinin tag followed by a linker consisting of two glycines and
452 a modified PAM sequence. The donor sequence was flanked by 60 bp homology arms on both
453 sides. Cas9 together with the gRNA and ssDNA donor were co-injected into C57BL/6 mouse
454 embryos at a single cell stage at the University of California, San Francisco Transgenic Gene
455 Targeting Core.

456

457 **Molecular biology**

458 SCAMP5-specific small hairpin RNA (shRNA) was designed with the aid of the InvivoGen siRNA
459 Wizard Online Tool to target the mouse SCAMP5 cDNA sequence. SCAMP5 knock-down
460 (TGCTCTTAGCATGGTTCATAA) and a scrambled control sequences were inserted into the
461 pLKO.1 lentiviral vector[99] obtained from Addgene using AgeI and EcoRI restriction sites. An
462 shRNA-resistant SCAMP5 rescue sequence was designed with the help of the Java Codon
463 Optimization Tool, effectively creating silent mutations in the target region sequence which would
464 be unrecognizable by the shRNA but would still code for SCAMP5. A custom lentiviral vector was
465 ordered through Vector Builder and includes the human synapsin promoter, SCAMP5 rescue
466 sequence, and mCherry to mark infected cells.

467

468 **Lentivirus production**

469 Low-passage LentiX HEK cells (Takara, cat. # 632180) were seeded onto 6-well plates and
470 transfected the following day with 1.5 µg of third-generation lentiviral vector FUGW encoding the
471 gene of interest together with 0.5 µg each of packaging plasmids pRRE, pVSVG and pRSV-Rev
472 using the FuGene HD transfection reagent (Promega, cat. # E2311) according to manufacturer's
473 instructions. Next morning, culture medium was changed into fresh Neurobasal. Viral supernatant
474 was collected 47 hours after transfection and concentrated 10x using Lenti-X Concentrator
475 (Takara, cat. # 631231). Aliquots were stored at -80C until use.
476
477 **Primary neuron culture**
478 Hippocampal neurons: Hippocampi were dissected from P0 mice of both sexes in Hank's
479 Balanced Salt Solution (HBSS) containing 10 mM HEPES and 20 mM glucose, dissociated in
480 0.25% trypsin, washed three times with Minimal Essential Medium containing 1x B27 (GIBCO,
481 17504-044), 2 mM glutamax (GIBCO, 35050-061), 5% FBS (HyClone, defined), 21 mM glucose
482 (Sigma, G8769) and 1x penicillin/streptomycin (Corning, 30-002-CL), triturated and plated on
483 poly-L-lysine coated coverslips at 350 cells/mm2 in the above Minimal Essential Media. After one
484 day *in vitro* (DIV1), 3/4 of the medium was changed to Neurobasal (GIBCO, 21103-049) with B27,
485 glutamax and penicillin/streptomycin. Cells were infected with lentiviruses encoding VGLUT2-
486 pHluorin, VMAT2-pHluorin, and/or shRNA SCAMP5 KD, scramble or rescue on DIV 4-5. 4 µM
487 cytosine arabinoside was added on DIV7 to inhibit glial proliferation.
488 Dopamine neurons: Ventral midbrain regions containing substantia nigra and ventral tegmental
489 area were dissected from neonatal HA-VMAT2 KI mice of both sexes. Tissue pieces were
490 dissected in Hank's Balanced Salt Solution (HBSS) containing 10 mM HEPES and 20 mM
491 glucose, dissociated in papain (Worthington) for 15 minutes, washed with media containing 60%
492 Neurobasal-A, 30% Basal Media Eagle, 10% fetal bovine serum (HyClone, defined), 1x B27,
493 2 mM GlutaMAX, 10 ng/mL glial cell line-derived neurotrophic factor (Millipore, MA, USA) and 1x
494 penicillin/streptomycin, triturated and plated in the above media at 1500 cells/mm^2.
495
496 **Synaptic Vesicle Preparation**
497 Whole brains or striatal tissue from 10-15 HA-VMAT2 KI mice was pooled per replicate. Tissue
498 was homogenized by 9 strokes at 900 rpm in cold homogenization buffer (0.3M sucrose, 1mM
499 Mg-EGTA, 10 mM HEPES-Tris, pH 7.4) with cOmplete protease inhibitors (Roche, cat. #
500 11836170001) using a glass teflon homogenizer. The homogenate (H) was centrifuged at 871 g
501 for 10 min at 4 °C in an SS34 rotor (Sorvall). Pellet was discarded and supernatant (S1) was

502 sedimented at 12,000 g for 15 min at 4 °C in an SS34 rotor. Both pellet P2 and supernatant S2
503 were collected and processed in parallel.
504 Pellet (P2) that is enriched in synaptosomes was resuspended in 10 mL homogenization buffer.
505 Resuspended P2 was sedimented at 14,500 g for 15 min at 4 °C in an SS34 rotor, the supernatant
506 (S2′) was removed and pooled with S2. P2′ was resuspended in 1.2 mL homogenization buffer
507 and then subjected to osmotic lysis for 45 min in 13.5 ml cold water with 8 mM HEPES-Tris, pH
508 7.4. The lysed P2′ was homogenized using five strokes at 3,000 rpm and centrifuged at 32,500 g
509 for 20 min. The lysed supernatant (LS1) was transferred into a new ultracentrifuge tube and
510 centrifuged at 280,000 g for 2 h using a Beckman 70 Ti rotor. Supernatant was discarded and
511 pellet (LP2) was resuspended in salt buffer (150 mM NaCl, 1 mM Mg-EGTA, 10 mM HEPES, pH
512 7.4) by repeated pipetting.
513 The S2/S2' samples were homogenized by 5 strokes at 3000 rpm and sedimented 32,500 g for
514 20 min. The resulting supernatant S3 was transferred to a new ultracentrifuge tube and
515 centrifuged at 280,000 g for 2 h using a Beckman 70 Ti rotor. Supernatant S4 was discarded and
516 pellet P4 was collected and resuspended in salt buffer like LP2 described above.
517 To obtain pure SVs, LP2 and P4 fractions were further purified by velocity sedimentation through
518 a continuous 5–25% glycerol gradient at 270,000 g for 1 h and 4 min in a Beckman SW 41 rotor.
519 0.5 mL fractions were collected from top to bottom. Fractions 7-12 were pooled and dialyzed over
520 night at 4C in 150 mM NaCl, 1 mM Mg-EGTA, 10 mM HEPES, pH 7.4.
521
522 **Immunoisolation**
523 Dialyzed synaptic vesicles were supplemented with 1% lysine and 1% glycine to reduce non-
524 specific binding and cOmplete protease inhibitors (Roche, cat. # 11836170001). Vesicles were
525 incubated on the rotator with anti-HA (Cell Signaling, Cat # 3724 for whole brain samples and
526 Covance, AB_291262 for striatal samples), anti-VGLUT2 (Synaptic Systems, cat. # 95E11)
527 antibodies for 2 hours at 4C. 5 µL of antibody was added per 2 mL of vesicle suspension.
528 In parallel, equal volumes of Dynabeads with protein A (Invitrogen 10001D) and protein G
529 (Invitrogen 10003D) were washed three times in salt buffer with protease inhibitors and
530 lysine/glycine. 50 µL of protein A/G beads was then added to 2 mL of synaptic vesicle/antibody
531 mix and incubated on the rotator for 1 hour at 4C. Beads were washed three times in salt buffer
532 and stored at -80C until processing for mass spectrometry.
533
534 **Mass Spectrometry**

535 Peptide and protein identification and TMT quantitation: Peak lists were generated using the
536 PAVA in-house software[100]. All generated peak lists were searched against the mouse subset of
537 the SwissProt database (SwissProt.2019.07.31, 17,026 entries searched) using Protein
538 Prospector[101] with the following parameters: Enzyme specificity was set as Trypsin, and up to 2
539 missed cleavages per peptide were allowed. Carbamidomethylation of cysteine residues, and
540 TMTPro16plex labeling of lysine residues and N-terminus of the protein were allowed as fixed
541 modifications. N-acetylation of the N-terminus of the protein, loss of protein N-terminal
542 methionine, pyroglutamate formation from of peptide N-terminal glutamines, and oxidation of
543 methionine were allowed as variable modifications Mass tolerance was 5 ppm in MS and 30 ppm
544 in MS/MS. The false discovery rate was estimated by searching the data using a concatenated
545 database which contains the original SwissProt database, as well as a version of each original
546 entry where the sequence has been randomized. A 1% FDR was permitted at the protein and
547 peptide level.
548 For quantitation, only unique peptides were considered. Relative quantization of peptide
549 abundance was performed by calculating the intensity of reporter ions corresponding to the
550 different TMT labels present in MS/MS spectra. Intensities were determined by Protein
551 Prospector. Median intensities of the reporter ions for all peptide spectral matches (PSMs) on
552 each TMT channel were used to normalize individual (sample-specific) intensity values. In
553 addition to classical SV proteins, we detected peptides associated with frequent contaminants of
554 SV preparations (proteasomes, ribosomes). To improve detection of differences in SV proteins,
555 contaminants associated with other organelles were excluded from analysis. For each PSM,
556 relative abundances were calculated as ratios of signal in VGLUT2 versus matching VMAT2
557 samples. For relative amounts of total protein, peptide ratios were aggregated to the protein levels
558 using median values of the log 2 ratios. Statistical significance was determined comparing the
559 log2 ratios to a log2 reference value of 0 using a two-tailed t-test.
560
561 **Western blot**
562 Proteins were separated by electrophoresis on 4-20% precast polyacrylamide gels (Bio-Rad) and
563 transferred to nitrocellulose membranes. Membranes were blocked in 5% milk tris buffered saline
564 with 0.1% Tween. Primary antibodies were incubated overnight at 4C and IRDye 680- or IRDye
565 800-coupled secondary antibodies (Rockland Immunochemicals) for 1 hour at room temperature.
566
567 **Immunohistochemistry**

568 To obtain fixed brain, mice were perfused with cold PBS, followed by 4% PFA in PBS. Brains
569 were postfixed overnight in 4% PFA and cryoprotected in PBS containing 30% sucrose. 35 µm
570 sections were cut using a Leica CM3050 S cryostat and floating sections were stored in PBS with
571 0.02% Na-azide. Cultured cells were fixed for 15 minutes in 4% PFA in PBS and washed three
572 times in PBS. Floating sections as well as cultured cells were blocked and permeabilized in PBS
573 containing 5% normal goat serum and 0.2% Triton X-100. Primary and secondary antibodies were
574 diluted in PBS containing 2.5% normal goat serum and 0.2% Triton X-100 in PBS for staining
575 slices and in 2.5% normal goat serum in PBS for staining cultured cells. Primary antibodies were
576 incubated overnight at 4°C for tissue sections and 2 hours at room temperature for cultured cells.
577 Secondary antibodies were incubated with tissue sections for 2 hours and cultured cells for 1 hour
578 in the dark at room temperature. Slices were mounted in Fluoromount-G (SouthernBiotech) or
579 Vectashield (Vector Laboratories). Antibodies were used at the following dilutions:
580
581 SYT1 Ms 1:5000 Synaptic Systems 105011
582 TH Ms 1:1000 EMD Millipore MAB5280
583 VG2 Gp 1:1000 Synaptic Systems 135404
584 VG2 Ch 1:1000 Synaptic Systems 135416
585 SYT2 Gp 1:1000 Synaptic Systems 105225
586 HA Rt 1:500 Roche 11867423001
587 SYPH Ms 1:500 Synaptic Systems 101011
588 SYPH Gp 1:100 Synaptic Systems 101 308
589 VAMP2 Rb 1:500 Synaptic Systems 104202
590 CSP Rb 1:500 Synaptic Systems 154003
591 SLC10a4 Rb 1:200 Sigma HPA028835
592 SYG Rb 1:100 Synaptic Systems 103002
593 SCAMP5 Rb 1:50 Invitrogen PA5-61269
594 All secondary antibodies were used at 1/750 dilution.
595
596 **Imaging of fixed cultures and brain slices**
597 Images of fixed cultured neurons and brain slices were acquired using the Nikon Eclipse Ti2-E
598 Microscope equipped with AR or AX confocal, AR1-DUG2 scan head with gallium arsenide
599 phosphide detector unit and a Plan Apo VC 60x DIC N2 oil objective. Lasers (405 nm, 488 nm,
600 561 nm and 640 nm) were used for excitation and ET525/50, ET593/46 and ET700/75 filters for
601 emission. Colocalization within release sites of dopamine/glutamate coreleasing neurons was

602 quantified on images acquired on a Nikon Eclipse Ti2-E microscope equipped with a AX confocal
603 module and a NSPARC (Nikon Spatial Array Confocal) detector[60]. Lense alignment was re-
604 calibrated every 45 minutes during imaging. Deconvolution was performed using Nikon's built-in
605 deblurring algorithm.
606
607 **Tissue Section 3D Analysis:** Presynaptic protein abundance in brain slices was quantified using
608 Imaris software (Oxford Instruments). Z stacks were acquired with a z-step of 0.125 µm and 3D
609 surfaces were generated based on HA-VMAT2 and VGLUT2 signal. Thresholds for surfaces were
610 selected manually and kept consistent within-mouse for all analyses. For Syt-2 colocalization
611 analysis, surfaces were generated manually and kept consistent within-mouse except for images
612 of the lateral geniculate nucleus, where the morphology of VGLUT2 presynapses departed
613 considerably from all other regions and unique thresholds were used. Mean signal for the protein
614 of interest was measured in HA-VMAT2 versus VGLUT2 surfaces and obtained values were
615 compared within image, and a paired t-test was applied for both slice- and mouse-level statistics.
616
617 **Image analysis in fixed cultures**
618 Presynaptic protein abundance in midbrain cultures was quantified in imageJ. Regions of interest
619 (ROI) were selected based on HA-VMAT2 or VGLUT2 signal or by the presence of both
620 transporters. The fluorescence intensity of proteins of interest was measured in the three sets of
621 ROIs. For colocalization analysis in dopamine/glutamate coreleasing neurons, images were
622 processed using the Coloc2 plugin in imageJ.
623
624 **Live imaging**
625 Hippocampal cultures between 16-19 DIV were mounted in a laminar flow perfusion and
626 stimulation chamber (Warner Instruments RC-21BRFS) on an inverted Nikon Eclipse Ti
627 fluorescence microscope, Hamamatsu ORCA-Flash4.0 camera, and Nikon Plan Apo λD 60x oil
628 objective. Fluorescence signals were collected under epifluorescence illumination using 465/95
629 nm excitation and 515/55 nm emission for pHluorin. Action potentials (APs) were evoked by
630 passing 1 ms bipolar current pulses through platinum electrodes, to yield fields of 5–10 V/cm.
631 Cells were continuously perfused with Tyrode's buffer (119 mM NaCl, 25 mM HEPES, 2 mM
632 $CaCl_2$, 2 mM $MgCl_2$, 2.5 mM KCl, and 30 mM glucose at pH 7.4) containing 10 µM 6-cyano-7-
633 nitroquinoxaline-2,3-dione (CNQX) and 10 µM 3-(2-carboxypiperazin-4-yl)propyl-1-phosphonic
634 acid (APV). Total cellular pHluorin content was revealed by applying Tyrode's buffer with 50 mM
635 NH_4Cl, where NaCl was reduced to 69 mM. Imaging was done at 37°C. For analysis, synaptic

636 boutons were selected manually. Background fluorescence was subtracted and fluorescence
637 intensity in the synaptic boutons was normalized to pre-stimulation baseline and to unquenched
638 (total) pHluorin fluorescence in NH_4Cl.
639
640 **Statistics**
641 Statistical analysis was performed using GraphPad Prism 10 software. The Shapiro-Wilk test was
642 used to assess the normal distribution of data. For comparing two conditions, two-tailed paired or
643 unpaired t-test (indicated in text and figure legends) was used if data was normally distributed
644 and Mann-Whitney test was used if data that did not pass the test for normality. One-way ANOVA
645 with Tukey's post hoc test was used for comparing more than two samples. Data are presented
646 as mean ± SEM and statistical significance as * $P < 0.05$, ** $P < 0.01$, *** $P < 0.001$, and **** $P <$
647 0.0001.

648 **ACKNOWLEDGEMENTS**

649 This work was supported by grants from the Brain and Behavior Research Foundation (29845)
650 and The Larry L. Hillblom Foundation (2022-A-004-SUP) as well as start-up funds from the
651 Cedars-Sinai Medical Center to K.S. R.H.E. is supported by R01NS103938 and R01NS129803
652 from the National Institute of Neurological Disorders and Stroke. We are grateful for imaging
653 support from V. Krishnan Ramanujan and Mingtian Che from the Cedars-Sinai Biobank and
654 Research Pathology Resource. Mass spectrometry was performed at the Mass Spectrometry
655 Resource at UCSF, which is supported by the Dr. Miriam and Sheldon G. Adelson Medical
656 Research Foundation (J.A.O.-P. & A.L.B.).

657 **AUTHOR CONTRIBUTIONS**

658 K.S. and R.H.E. designed research; H.A., A.J.D., H.X., J.A.O.-P., J.A., A.S., B.G., N.C. and K.S.
659 performed experiments; H.A., A.J.D., H.X., J.A.O.-P., J.A., A.S., B.G. and K.S. analyzed data;
660 A.L.B, R.H.E. and K.S. acquired funding; K.S. wrote the paper with feedback from R.H.E., H.A.,
661 A.J.D., H.X., J.A.O.-P. and A.S.

662 **COMPETING INTERESTS**

663 R.H.E. is a consultant for Nine Square Therapeutics. Other authors have no competing interests
664 to declare.
665
666

667 **REFERENCES**
668

669 1. Takamori, S., Holt, M., Stenius, K., Lemke, E.A., Grønborg, M., Riedel, D., Urlaub, H., Schenck,
670 S., Brügger, B., Ringler, P., et al. (2006). Molecular Anatomy of a Trafficking Organelle. Cell *127*,
671 831–846. https://doi.org/10.1016/j.cell.2006.10.030.

672 2. Südhof, T.C., and Rothman, J.E. (2009). Membrane Fusion: Grappling with SNARE and SM
673 Proteins. Science *323*, 474–477. https://doi.org/10.1126/science.1161748.

674 3. Südhof, T.C. (2012). The Presynaptic Active Zone. Neuron *75*, 11–25.
675 https://doi.org/10.1016/j.neuron.2012.06.012.

676 4. Markram, H., Wang, Y., and Tsodyks, M. (1998). Differential signaling via the same axon of
677 neocortical pyramidal neurons. Proc National Acad Sci *95*, 5323–5328.
678 https://doi.org/10.1073/pnas.95.9.5323.

679 5. Ding, J., Peterson, J.D., and Surmeier, D.J. (2008). Corticostriatal and thalamostriatal synapses
680 have distinctive properties. J Neurosci Official J Soc Neurosci *28*, 6483–6492.
681 https://doi.org/10.1523/jneurosci.0435-08.2008.

682 6. Scanziani, M., Gähwiler, B.H., and Charpak, S. (1998). Target cell-specific modulation of
683 transmitter release at terminals from a single axon. Proc. Natl. Acad. Sci. *95*, 12004–12009.
684 https://doi.org/10.1073/pnas.95.20.12004.

685 7. Dittman, J.S., Kreitzer, A.C., and Regehr, W.G. (2000). Interplay between Facilitation,
686 Depression, and Residual Calcium at Three Presynaptic Terminals. J. Neurosci. *20*, 1374–1385.
687 https://doi.org/10.1523/jneurosci.20-04-01374.2000.

688 8. Neher, E. (2015). Merits and Limitations of Vesicle Pool Models in View of Heterogeneous
689 Populations of Synaptic Vesicles. Neuron *87*, 1131–1142.
690 https://doi.org/10.1016/j.neuron.2015.08.038.

691 9. Schikorski, T., and Stevens, C.F. (2001). Morphological correlates of functionally defined
692 synaptic vesicle populations. Nat. Neurosci. *4*, 391–395. https://doi.org/10.1038/86042.

693 10. Chamberland, S., and Tóth, K. (2016). Functionally heterogeneous synaptic vesicle pools
694 support diverse synaptic signalling. J. Physiol. *594*, 825–835. https://doi.org/10.1113/jp270194.

695 11. Atwood, H.L., and Karunanithi, S. (2002). Diversification of synaptic strength: presynaptic
696 elements. Nat. Rev. Neurosci. *3*, 497–516. https://doi.org/10.1038/nrn876.

697 12. Asmerian, H., Alberts, J., Sanetra, A.M., Diaz, A.J., and Silm, K. (2024). Role of adaptor
698 protein complexes in generating functionally distinct synaptic vesicle pools. J. Physiol.
699 https://doi.org/10.1113/jp286179.

700 13. Saunders, A., Macosko, E.Z., Wysoker, A., Goldman, M., Krienen, F.M., Rivera, H. de, Bien,
701 E., Baum, M., Bortolin, L., Wang, S., et al. (2018). Molecular Diversity and Specializations among

the Cells of the Adult Mouse Brain. Cell *174*, 1015-1030.e16. https://doi.org/10.1016/j.cell.2018.07.028.

14. Yao, Z., Velthoven, C.T.J. van, Kunst, M., Zhang, M., McMillen, D., Lee, C., Jung, W., Goldy, J., Abdelhak, A., Aitken, M., et al. (2023). A high-resolution transcriptomic and spatial atlas of cell types in the whole mouse brain. Nature *624*, 317–332. https://doi.org/10.1038/s41586-023-06812-z.

15. Siletti, K., Hodge, R., Albiach, A.M., Lee, K.W., Ding, S.-L., Hu, L., Lönnerberg, P., Bakken, T., Casper, T., Clark, M., et al. (2023). Transcriptomic diversity of cell types across the adult human brain. Science *382*, eadd7046. https://doi.org/10.1126/science.add7046.

16. Oostrum, M. van, Blok, T.M., Giandomenico, S.L., Dieck, S. tom, Tushev, G., Fürst, N., Langer, J.D., and Schuman, E.M. (2023). The proteomic landscape of synaptic diversity across brain regions and cell types. Cell. https://doi.org/10.1016/j.cell.2023.09.028.

17. Branco, T., and Staras, K. (2009). The probability of neurotransmitter release: variability and feedback control at single synapses. Nat. Rev. Neurosci. *10*, 373–383. https://doi.org/10.1038/nrn2634.

18. Descarries, L., and Mechawar, N. (2000). Ultrastructural evidence for diffuse transmission by monoamine and acetylcholine neurons of the central nervous system. Prog Brain Res *125*, 27–47. https://doi.org/10.1016/s0079-6123(00)25005-x.

19. Beaulieu, J.-M., and Gainetdinov, R.R. (2011). The Physiology, Signaling, and Pharmacology of Dopamine Receptors. Pharmacol. Rev. *63*, 182–217. https://doi.org/10.1124/pr.110.002642.

20. Schultz, W., Dayan, P., and Montague, P.R. (1997). A Neural Substrate of Prediction and Reward. Science *275*, 1593–1599. https://doi.org/10.1126/science.275.5306.1593.

21. Pan, P.-Y., and Ryan, T.A. (2012). Calbindin controls release probability in ventral tegmental area dopamine neurons. Nat Neurosci *15*, 813–815. https://doi.org/10.1038/nn.3099.

22. Silm, K., Yang, J., Marcott, P.F., Asensio, C.S., Eriksen, J., Guthrie, D.A., Newman, A.H., Ford, C.P., and Edwards, R.H. (2019). Synaptic Vesicle Recycling Pathway Determines Neurotransmitter Content and Release Properties. Neuron *102*, 786-800.e5. https://doi.org/10.1016/j.neuron.2019.03.031.

23. Pereira, D.B., Schmitz, Y., Mészáros, J., Merchant, P., Hu, G., Li, S., Henke, A., Lizardi-Ortiz, J.E., Karpowicz, R.J., Morgenstern, T.J., et al. (2016). Fluorescent false neurotransmitter reveals functionally silent dopamine vesicle clusters in the striatum. Nat Neurosci *19*, 578–586. https://doi.org/10.1038/nn.4252.

24. Liu, C., Kershberg, L., Wang, J., Schneeberger, S., and Kaeser, P.S. (2018). Dopamine Secretion Is Mediated by Sparse Active Zone-like Release Sites. Cell *172*, 706-718.e15. https://doi.org/10.1016/j.cell.2018.01.008.

25. Banerjee, A., Imig, C., Balakrishnan, K., Kershberg, L., Lipstein, N., Uronen, R.-L., Wang, J., Cai, X., Benseler, F., Rhee, J.S., et al. (2022). Molecular and functional architecture of striatal

739 dopamine release sites. Neuron, 2020.11.25.398255.
740 https://doi.org/10.1016/j.neuron.2021.10.028.

741 26. Kershberg, L., Banerjee, A., and Kaeser, P.S. (2022). Protein composition of axonal dopamine
742 release sites in the striatum. eLife *11*, e83018. https://doi.org/10.7554/elife.83018.

743 27. Jain, S., Yee, A.G., Maas, J., Gierok, S., Xu, H., Stansil, J., Eriksen, J., Nelson, A.B., Silm,
744 K., Ford, C.P., et al. (2023). Adaptor protein-3 produces synaptic vesicles that release phasic
745 dopamine. Proc. Natl. Acad. Sci. United States Am. *120*, e2309843120.
746 https://doi.org/10.1073/pnas.2309843120.

747 28. Voglmaier, S.M., Kam, K., Yang, H., Fortin, D.L., Hua, Z., Nicoll, R.A., and Edwards, R.H.
748 (2006). Distinct Endocytic Pathways Control the Rate and Extent of Synaptic Vesicle Protein
749 Recycling. Neuron *51*, 71–84. https://doi.org/10.1016/j.neuron.2006.05.027.

750 29. Kim, S.H., and Ryan, T.A. (2009). Synaptic vesicle recycling at CNS snapses without AP-2.
751 J. Neurosci.: Off. J. Soc. Neurosci. *29*, 3865–3874. https://doi.org/10.1523/jneurosci.5639-
752 08.2009.

753 30. Xu, H., Oses-Prieto, J.A., Khvotchev, M., Jain, S., Liang, J., Burlingame, A., and Edwards,
754 R.H. (2023). Adaptor protein AP-3 produces synaptic vesicles that release at high frequency by
755 recruiting phospholipid flippase ATP8A1. Nat. Neurosci., 1–16. https://doi.org/10.1038/s41593-
756 023-01434-0.

757 31. Lavoie, N., Jeyaraju, D.V., Peralta, M.R., Seress, L., Pellegrini, L., and Tóth, K. (2011).
758 Vesicular Zinc Regulates the Ca 2+ Sensitivity of a Subpopulation of Presynaptic Vesicles at
759 Hippocampal Mossy Fiber Terminals. J. Neurosci. *31*, 18251–18265.
760 https://doi.org/10.1523/jneurosci.4164-11.2011.

761 32. Hnasko, T.S., Chuhma, N., Zhang, H., Goh, G.Y., Sulzer, D., Palmiter, R.D., Rayport, S., and
762 Edwards, R.H. (2010). Vesicular Glutamate Transport Promotes Dopamine Storage and
763 Glutamate Corelease In Vivo. Neuron *65*, 643–656. https://doi.org/10.1016/j.neuron.2010.02.012.

764 33. Stuber, G.D., Hnasko, T.S., Britt, J.P., Edwards, R.H., and Bonci, A. (2010). Dopaminergic
765 Terminals in the Nucleus Accumbens But Not the Dorsal Striatum Corelease Glutamate. J
766 Neurosci *30*, 8229–8233. https://doi.org/10.1523/jneurosci.1754-10.2010.

767 34. Chuhma, N., Mingote, S., Moore, H., and Rayport, S. (2014). Dopamine Neurons Control
768 Striatal Cholinergic Neurons via Regionally Heterogeneous Dopamine and Glutamate Signaling.
769 Neuron *81*, 901–912. https://doi.org/10.1016/j.neuron.2013.12.027.

770 35. Gan, Q., and Watanabe, S. (2018). Synaptic Vesicle Endocytosis in Different Model Systems.
771 Front Cell Neurosci *12*, 171. https://doi.org/10.3389/fncel.2018.00171.

772 36. Weston, M.C., Nehring, R.B., Wojcik, S.M., and Rosenmund, C. (2011). Interplay between
773 VGLUT Isoforms and Endophilin A1 Regulates Neurotransmitter Release and Short-Term
774 Plasticity. Neuron *69*, 1147–1159. https://doi.org/10.1016/j.neuron.2011.02.002.

775 37. Jr., R.T.F., Kam, K., Qureshi, T., Johnson, J., Copenhagen, D.R., Storm-Mathisen, J.,
776 Chaudhry, F.A., Nicoll, R.A., and Edwards, R.H. (2004). Vesicular Glutamate Transporters 1 and
777 2 Target to Functionally Distinct Synaptic Release Sites. Science *304*, 1815–1819.
778 https://doi.org/10.1126/science.1097468.

779 38. Gronborg, M., Pavlos, N.J., Brunk, I., Chua, J.J.E., Munster-Wandowski, A., Riedel, D.,
780 Ahnert-Hilger, G., Urlaub, H., and Jahn, R. (2010). Quantitative Comparison of Glutamatergic and
781 GABAergic Synaptic Vesicles Unveils Selectivity for Few Proteins Including MAL2, a Novel
782 Synaptic Vesicle Protein. J Neurosci *30*, 2–12. https://doi.org/10.1523/jneurosci.4074-09.2010.

783 39. Yang, H., Wang, H., and Jaenisch, R. (2014). Generating genetically modified mice using
784 CRISPR/Cas-mediated genome engineering. Nat. Protoc. *9*, 1956–1968.
785 https://doi.org/10.1038/nprot.2014.134.

786 40. Huttner, W.B., Schiebler, W., Greengard, P., and Camilli, P.D. (1983). Synapsin I (protein I),
787 a nerve terminal-specific phosphoprotein. III. Its association with synaptic vesicles studied in a
788 highly purified synaptic vesicle preparation. J Cell Biology *96*, 1374–1388.
789 https://doi.org/10.1083/jcb.96.5.1374.

790 41. Zhang, S., Qi, J., Li, X., Wang, H.-L., Britt, J.P., Hoffman, A.F., Bonci, A., Lupica, C.R., and
791 Morales, M. (2015). Dopaminergic and glutamatergic microdomains in a subset of rodent
792 mesoaccumbens axons. Nat Neurosci *18*, 386–392. https://doi.org/10.1038/nn.3945.

793 42. Lapios, P., Anger, R., Paget-Blanc, V., Marza, E., Lučić, V., Fronzes, R., Herzog, E., and
794 Perrais, D. (2025). Cryo-correlative light and electron tomography of dopaminergic axonal
795 varicosities reveals non-synaptic modulation of cortico-striatal synapses. bioRxiv,
796 2025.02.07.637058. https://doi.org/10.1101/2025.02.07.637058.

797 43. Larhammar, M., Patra, K., Blunder, M., Emilsson, L., Peuckert, C., Arvidsson, E., Rönnlund,
798 D., Preobraschenski, J., Birgner, C., Limbach, C., et al. (2015). SLC10A4 Is a Vesicular Amine-
799 Associated Transporter Modulating Dopamine Homeostasis. Biol Psychiat *77*, 526–536.
800 https://doi.org/10.1016/j.biopsych.2014.07.017.

801 44. Amilhon, B., Lepicard, È., Renoir, T., Mongeau, R., Popa, D., Poirel, O., Miot, S., Gras, C.,
802 Gardier, A.M., Gallego, J., et al. (2010). VGLUT3 (Vesicular Glutamate Transporter Type 3)
803 Contribution to the Regulation of Serotonergic Transmission and Anxiety. J Neurosci *30*, 2198–
804 2210. https://doi.org/10.1523/jneurosci.5196-09.2010.

805 45. Kaeser-Woo, Y.J., Younts, T.J., Yang, X., Zhou, P., Wu, D., Castillo, P.E., and Südhof, T.C.
806 (2013). Synaptotagmin-12 Phosphorylation by cAMP-Dependent Protein Kinase Is Essential for
807 Hippocampal Mossy Fiber LTP. J Neurosci *33*, 9769–9780.
808 https://doi.org/10.1523/jneurosci.5814-12.2013.

809 46. Maximov, A., Shin, O.-H., Liu, X., and Südhof, T.C. (2007). Synaptotagmin-12, a synaptic
810 vesicle phosphoprotein that modulates spontaneous neurotransmitter release. J Cell Biology *176*,
811 113–124. https://doi.org/10.1083/jcb.200607021.

812 47. Xu, J., Mashimo, T., and Südhof, T.C. (2007). Synaptotagmin-1, -2, and -9: Ca2+ Sensors for
813 Fast Release that Specify Distinct Presynaptic Properties in Subsets of Neurons. Neuron *54*, 567–
814 581. https://doi.org/10.1016/j.neuron.2007.05.004.

815 48. Meijer, M., Öttl, M., Yang, J., Subkhangulova, A., Kumar, A., Feng, Z., Voorst, T.W. van,
816 Groffen, A.J., Weering, J.R.T. van, Zhang, Y., et al. (2024). Tomosyns attenuate SNARE
817 assembly and synaptic depression by binding to VAMP2-containing template complexes. Nat.
818 Commun. *15*, 2652. https://doi.org/10.1038/s41467-024-46828-1.

819 49. Sauvola, C.W., Akbergenova, Y., Cunningham, K.L., Aponte-Santiago, N.A., and Littleton,
820 J.T. (2021). The decoy SNARE Tomosyn sets tonic versus phasic release properties and is
821 required for homeostatic synaptic plasticity. eLife *10*, e72841. https://doi.org/10.7554/elife.72841.

822 50. Arkan, S., Ljungberg, M., Kirik, D., and Hansen, C. (2021). DNAJB6 suppresses alpha-
823 synuclein induced pathology in an animal model of Parkinson's disease. Neurobiol. Dis. *158*,
824 105477. https://doi.org/10.1016/j.nbd.2021.105477.

825 51. Aprile, F.A., Källstig, E., Limorenko, G., Vendruscolo, M., Ron, D., and Hansen, C. (2017).
826 The molecular chaperones DNAJB6 and Hsp70 cooperate to suppress α-synuclein aggregation.
827 Sci Rep-uk *7*, 9039. https://doi.org/10.1038/s41598-017-08324-z.

828 52. Ng, J., Cortès-Saladelafont, E., Abela, L., Termsarasab, P., Mankad, K., Sudhakar, S.,
829 Gorman, K.M., Heales, S.J.R., Pope, S., Biassoni, L., et al. (2020). DNAJC6 Mutations Disrupt
830 Dopamine Homeostasis in Juvenile Parkinsonism-Dystonia. Mov. Disord. *35*, 1357–1368.
831 https://doi.org/10.1002/mds.28063.

832 53. Fjorback, A.W., Müller, H.K., Haase, J., Raarup, M.K., and Wiborg, O. (2011). Modulation of
833 the dopamine transporter by interaction with Secretory Carrier Membrane Protein 2. Biochem.
834 Biophys. Res. Commun. *406*, 165–170. https://doi.org/10.1016/j.bbrc.2011.01.069.

835 54. Cheramy, A., Leviel, V., and Glowinski, J. (1981). Dendritic release of dopamine in the
836 substantia nigra. Nature *289*, 537–543. https://doi.org/10.1038/289537a0.

837 55. Nirenberg, M.J., Chan, J., Liu, Y., Edwards, R.H., and Pickel, V.M. (1996). Ultrastructural
838 Localization of the Vesicular Monoamine Transporter-2 in Midbrain Dopaminergic Neurons:
839 Potential Sites for Somatodendritic Storage and Release of Dopamine. J. Neurosci. *16*, 4135–
840 4145. https://doi.org/10.1523/jneurosci.16-13-04135.1996.

841 56. Burger, S., Döring, B., Hardt, M., Beuerlein, K., Gerstberger, R., and Geyer, J. (2011). Co-
842 expression studies of the orphan carrier protein Slc10a4 and the vesicular carriers VAChT and
843 VMAT2 in the rat central and peripheral nervous system. Neuroscience *193*, 109–121.
844 https://doi.org/10.1016/j.neuroscience.2011.06.068.

845 57. Fremeau, R.T., Troyer, M.D., Pahner, I., Nygaard, G.O., Tran, C.H., Reimer, R.J., Bellocchio,
846 E.E., Fortin, D., Storm-Mathisen, J., and Edwards, R.H. (2001). The Expression of Vesicular
847 Glutamate Transporters Defines Two Classes of Excitatory Synapse. Neuron *31*, 247–260.
848 https://doi.org/10.1016/s0896-6273(01)00344-0.

849 58. Land, P.W., Kyonka, E., and Shamalla-Hannah, L. (2004). Vesicular glutamate transporters
850 in the lateral geniculate nucleus: expression of VGLUT2 by retinal terminals. Brain Res. *996*, 251–
851 254. https://doi.org/10.1016/j.brainres.2003.10.032.

852 59. Graziano, A., Liu, X., Murray, K.D., and Jones, E.G. (2008). Vesicular glutamate transporters
853 define two sets of glutamatergic afferents to the somatosensory thalamus and two thalamocortical
854 projections in the mouse. J Comp Neurol *507*, 1258–1276. https://doi.org/10.1002/cne.21592.

855 60. Delattre, S. (2023). Igniting New Confocal Imaging Potential – Nikon AX R Series with
856 NSPARC. Microsc. Today *31*, 23–27. https://doi.org/10.1093/mictod/qaad088.

857 61. Zhao, H., Kim, Y., Park, J., Park, D., Lee, S.-E., Chang, I., and Chang, S. (2014). SCAMP5
858 Plays a Critical Role in Synaptic Vesicle Endocytosis during High Neuronal Activity. J Neurosci
859 *34*, 10085–10095. https://doi.org/10.1523/jneurosci.2156-14.2014.

860 62. Park, D., Lee, U., Cho, E., Zhao, H., Kim, J.A., Lee, B.J., Regan, P., Ho, W.-K., Cho, K., and
861 Chang, S. (2018). Impairment of Release Site Clearance within the Active Zone by Reduced
862 SCAMP5 Expression Causes Short-Term Depression of Synaptic Release. Cell Reports *22*,
863 3339–3350. https://doi.org/10.1016/j.celrep.2018.02.088.

864 63. Miesenböck, G., Angelis, D.A.D., and Rothman, J.E. (1998). Visualizing secretion and
865 synaptic transmission with pH-sensitive green fluorescent proteins. Nature *394*, 192–195.
866 https://doi.org/10.1038/28190.

867 64. Paget-Blanc, V., Pfeffer, M.E., Pronot, M., Lapios, P., Angelo, M.-F., Walle, R., Cordelières,
868 F.P., Levet, F., Claverol, S., Lacomme, S., et al. (2022). A synaptomic analysis reveals dopamine
869 hub synapses in the mouse striatum. Nat Commun *13*, 3102. https://doi.org/10.1038/s41467-022-
870 30776-9.

871 65. Hobson, B.D., Choi, S.J., Mosharov, E.V., Soni, R.K., Sulzer, D., and Sims, P.A. (2022).
872 Subcellular proteomics of dopamine neurons in the mouse brain. Elife *11*, e70921.
873 https://doi.org/10.7554/elife.70921.

874 66. Dunn, A.R., Stout, K.A., Ozawa, M., Lohr, K.M., Hoffman, C.A., Bernstein, A.I., Li, Y., Wang,
875 M., Sgobio, C., Sastry, N., et al. (2017). Synaptic vesicle glycoprotein 2C (SV2C) modulates
876 dopamine release and is disrupted in Parkinson disease. Proc. Natl. Acad. Sci. *114*, E2253–
877 E2262. https://doi.org/10.1073/pnas.1616892114.

878 67. Bucher, M.L., Dunn, A.R., Bradner, J.M., Egerton, K.S., Burkett, J.P., Johnson, M.A., and
879 Miller, G.W. (2024). Synaptic vesicle glycoprotein 2C enhances vesicular storage of dopamine
880 and counters dopaminergic toxicity. Eur. J. Neurosci. *59*, 2483–2501.
881 https://doi.org/10.1111/ejn.16311.

882 68. Kim, S.-Y., Mori, T., Chek, M.F., Furuya, S., Matsumoto, K., Yajima, T., Ogura, T., and
883 Hakoshima, T. (2021). Structural insights into vesicle amine transport-1 (VAT-1) as a member of
884 the NADPH-dependent quinone oxidoreductase family. Sci. Rep. *11*, 2120.
885 https://doi.org/10.1038/s41598-021-81409-y.

886 69. Janz, R., Südhof, T.C., Hammer, R.E., Unni, V., Siegelbaum, S.A., and Bolshakov, V.Y.
887 (1999). Essential Roles in Synaptic Plasticity for Synaptogyrin I and Synaptophysin I. Neuron *24*,
888 687–700. https://doi.org/10.1016/s0896-6273(00)81122-8.

889 70. Raja, M.K., Preobraschenski, J., Olmo-Cabrera, S.D., Martinez-Turrillas, R., Jahn, R., Perez-
890 Otano, I., and Wesseling, J.F. (2019). Elevated synaptic vesicle release probability in

891 synaptophysin/gyrin family quadruple knockouts. Elife *8*, e40744.
892 https://doi.org/10.7554/elife.40744.

893 71. Pennuto, M., Bonanomi, D., Benfenati, F., and Valtorta, F. (2003). Synaptophysin I Controls
894 the Targeting of VAMP2/Synaptobrevin II to Synaptic Vesicles. Mol. Biol. Cell *14*, 4909–4919.
895 https://doi.org/10.1091/mbc.e03-06-0380.

896 72. Wang, C., Jiang, W., Leitz, J., Yang, K., Esquivies, L., Wang, X., Shen, X., Held, R.G., Adams,
897 D.J., Basta, T., et al. (2024). Structure and topography of the synaptic V-ATPase–synaptophysin
898 complex. Nature *631*, 899–904. https://doi.org/10.1038/s41586-024-07610-x.

899 73. Harper, C.B., Blumrich, E.-M., and Cousin, M.A. (2021). Synaptophysin controls
900 synaptobrevin-II retrieval via a cryptic C-terminal interaction site. J. Biol. Chem. *296*, 100266.
901 https://doi.org/10.1016/j.jbc.2021.100266.

902 74. Park, D., Fujise, K., Wu, Y., Luján, R., Olmo-Cabrera, S.D., Wesseling, J.F., and Camilli, P.D.
903 (2024). Overlapping role of synaptophysin and synaptogyrin family proteins in determining the
904 small size of synaptic vesicles. Proc. Natl. Acad. Sci. United States Am. *121*, e2409605121.
905 https://doi.org/10.1073/pnas.2409605121.

906 75. Preobraschenski, J., Kreutzberger, A.J.B., Ganzella, M., Münster-Wandowski, A.,
907 Kreutzberger, M.A.B., Oolsthorn, L.H.M., Seibert, S., Kiessling, V., Riedel, D., Witkowska, A., et
908 al. (2025). Synaptophysin accelerates synaptic vesicle fusion by expanding the membrane upon
909 neurotransmitter loading. Sci. Adv. *11*, eads4661. https://doi.org/10.1126/sciadv.ads4661.

910 76. Ruhl, D.A., Bomba-Warczak, E., Watson, E.T., Bradberry, M.M., Peterson, T.A., Basu, T.,
911 Frelka, A., Evans, C.S., Briguglio, J.S., Basta, T., et al. (2019). Synaptotagmin 17 controls neurite
912 outgrowth and synaptic physiology via distinct cellular pathways. Nat Commun *10*, 3532.
913 https://doi.org/10.1038/s41467-019-11459-4.

914 77. Dean, C., Dunning, F.M., Liu, H., Bomba-Warczak, E., Martens, H., Bharat, V., Ahmed, S.,
915 and Chapman, E.R. (2012). Axonal and dendritic synaptotagmin isoforms revealed by a pHluorin-
916 syt functional screen. Mol. Biol. Cell *23*, 1715–1727. https://doi.org/10.1091/mbc.e11-08-0707.

917 78. Delignat-Lavaud, B., Kano, J., Ducrot, C., Massé, I., Mukherjee, S., Giguère, N., Moquin, L.,
918 Lévesque, C., Burke, S., Denis, R., et al. (2023). Synaptotagmin-1-dependent phasic axonal
919 dopamine release is dispensable for basic motor behaviors in mice. Nat. Commun. *14*, 4120.
920 https://doi.org/10.1038/s41467-023-39805-7.

921 79. Lebowitz, J.J., Banerjee, A., Qiao, C., Bunzow, J.R., Williams, J.T., and Kaeser, P.S. (2023).
922 Synaptotagmin-1 is a Ca2+ sensor for somatodendritic dopamine release. Cell Rep. *42*, 111915.
923 https://doi.org/10.1016/j.celrep.2022.111915.

924 80. Chen, C., Arai, I., Satterfield, R., Young, S.M., and Jonas, P. (2017). Synaptotagmin 2 Is the
925 Fast Ca2+ Sensor at a Central Inhibitory Synapse. Cell Reports *18*, 723–736.
926 https://doi.org/10.1016/j.celrep.2016.12.067.

927 81. Kochubey, O., Babai, N., and Schneggenburger, R. (2016). A Synaptotagmin Isoform Switch
928 during the Development of an Identified CNS Synapse. Neuron *90*, 984–999.
929 https://doi.org/10.1016/j.neuron.2016.04.038.

930 82. Bouhours, B., Gjoni, E., Kochubey, O., and Schneggenburger, R. (2017). Synaptotagmin2
931 (Syt2) Drives Fast Release Redundantly with Syt1 at the Output Synapses of Parvalbumin-
932 Expressing Inhibitory Neurons. J Neurosci *37*, 4604–4617.
933 https://doi.org/10.1523/jneurosci.3736-16.2017.

934 83. Jong, A.P.H. de, Meijer, M., Saarloos, I., Cornelisse, L.N., Toonen, R.F.G., Sørensen, J.B.,
935 and Verhage, M. (2016). Phosphorylation of synaptotagmin-1 controls a post-priming step in PKC-
936 dependent presynaptic plasticity. Proc National Acad Sci *113*, 5095–5100.
937 https://doi.org/10.1073/pnas.1522927113.

938 84. Müller, H.K., Wiborg, O., and Haase, J. (2006). Subcellular Redistribution of the Serotonin
939 Transporter by Secretory Carrier Membrane Protein 2*. J. Biol. Chem. *281*, 28901–28909.
940 https://doi.org/10.1074/jbc.m602848200.

941 85. Lee, U., Choi, C., Ryu, S.H., Park, D., Lee, S.-E., Kim, K., Kim, Y., and Chang, S. (2021).
942 SCAMP5 plays a critical role in axonal trafficking and synaptic localization of NHE6 to adjust
943 quantal size at glutamatergic synapses. Proc National Acad Sci *118*, e2011371118.
944 https://doi.org/10.1073/pnas.2011371118.

945 86. Liao, H., Zhang, J., Shestopal, S., Szabo, G., Castle, A., and Castle, D. (2008). Nonredundant
946 function of secretory carrier membrane protein isoforms in dense core vesicle exocytosis. Am. J.
947 Physiol.-Cell Physiol. *294*, C797–C809. https://doi.org/10.1152/ajpcell.00493.2007.

948 87. Fernández-Chacón, R., Wölfel, M., Nishimune, H., Tabares, L., Schmitz, F., Castellano-
949 Muñoz, M., Rosenmund, C., Montesinos, M.L., Sanes, J.R., Schneggenburger, R., et al. (2004).
950 The Synaptic Vesicle Protein CSPα Prevents Presynaptic Degeneration. Neuron *42*, 237–251.
951 https://doi.org/10.1016/s0896-6273(04)00190-4.

952 88. Lopez-Ortega, E., Ruiz, R., and Tabares, L. (2017). CSPα, a Molecular Co-chaperone
953 Essential for Short and Long-Term Synaptic Maintenance. Front Neurosci-switz *11*, 39.
954 https://doi.org/10.3389/fnins.2017.00039.

955 89. Zhang, X.M., François, U., Silm, K., Angelo, M.F., Fernandez-Busch, M.V., Maged, M., Martin,
956 C., Bernard, V., Cordelières, F.P., Deshors, M., et al. (2019). A proline-rich motif on VGLUT1
957 reduces synaptic vesicle super-pool and spontaneous release frequency. Elife *8*, e50401.
958 https://doi.org/10.7554/elife.50401.

959 90. Gaffield, M.A., Rizzoli, S.O., and Betz, W.J. (2006). Mobility of Synaptic Vesicles in Different
960 Pools in Resting and Stimulated Frog Motor Nerve Terminals. Neuron *51*, 317–325.
961 https://doi.org/10.1016/j.neuron.2006.06.031.

962 91. Scheuber, A., Rudge, R., Danglot, L., Raposo, G., Binz, T., Poncer, J.-C., and Galli, T. (2006).
963 Loss of AP-3 function affects spontaneous and evoked release at hippocampal mossy fiber
964 synapses. Proc. Natl. Acad. Sci. *103*, 16562–16567. https://doi.org/10.1073/pnas.0603511103.

965 92. Newell-Litwa, K., Chintala, S., Jenkins, S., Pare, J.-F., McGaha, L., Smith, Y., and Faundez,
966 V. (2010). Hermansky-Pudlak Protein Complexes, AP-3 and BLOC-1, Differentially Regulate
967 Presynaptic Composition in the Striatum and Hippocampus. J. Neurosci. *30*, 820–831.
968 https://doi.org/10.1523/jneurosci.3400-09.2010.

969 93. Hua, Z., Leal-Ortiz, S., Foss, S.M., Waites, C.L., Garner, C.C., Voglmaier, S.M., and Edwards,
970 R.H. (2011). v-SNARE Composition Distinguishes Synaptic Vesicle Pools. Neuron *71*, 474–487.
971 https://doi.org/10.1016/j.neuron.2011.06.010.

972 94. Newell-Litwa, K., Salazar, G., Smith, Y., and Faundez, V. (2009). Roles of BLOC-1 and
973 Adaptor Protein-3 Complexes in Cargo Sorting to Synaptic Vesicles. Mol. Biol. Cell *20*, 1441–
974 1453. https://doi.org/10.1091/mbc.e08-05-0456.

975 95. Xie, Y.X., Naseri, N.N., Fels, J., Kharel, P., Na, Y., Lane, D., Burré, J., and Sharma, M. (2022).
976 Lysosomal exocytosis releases pathogenic α-synuclein species from neurons in synucleinopathy
977 models. Nat Commun *13*, 4918. https://doi.org/10.1038/s41467-022-32625-1.

978 96. Wang, G., Nola, S., Bovio, S., Bun, P., Coppey-Moisan, M., Lafont, F., and Galli, T. (2018).
979 Biomechanical Control of Lysosomal Secretion Via the VAMP7 Hub: A Tug-of-War between
980 VARP and LRRK1. iScience *4*, 127–143. https://doi.org/10.1016/j.isci.2018.05.016.

981 97. Binotti, B., Ninov, M., Cepeda, A.P., Ganzella, M., Matti, U., Riedel, D., Urlaub, H.,
982 Sambandan, S., and Jahn, R. (2023). ATG9 resides on a unique population of small vesicles in
983 presynaptic nerve terminals. Autophagy. https://doi.org/10.1080/15548627.2023.2274204.

984 98. Bolz, S., and Haucke, V. (2024). Biogenesis and reformation of synaptic vesicles. J. Physiol.
985 https://doi.org/10.1113/jp286554.

986 99. Moffat, J., Grueneberg, D.A., Yang, X., Kim, S.Y., Kloepfer, A.M., Hinkle, G., Piqani, B.,
987 Eisenhaure, T.M., Luo, B., Grenier, J.K., et al. (2006). A Lentiviral RNAi Library for Human and
988 Mouse Genes Applied to an Arrayed Viral High-Content Screen. Cell *124*, 1283–1298.
989 https://doi.org/10.1016/j.cell.2006.01.040.

990 100. Guan, S., Price, J.C., Prusiner, S.B., Ghaemmaghami, S., and Burlingame, A.L. (2011). A
991 Data Processing Pipeline for Mammalian Proteome Dynamics Studies Using Stable Isotope
992 Metabolic Labeling*. Mol. Cell. Proteom. *10*, M111.010728.
993 https://doi.org/10.1074/mcp.m111.010728.

994 101. Clauser, K.R., Baker, P., and Burlingame, A.L. (1999). Role of Accurate Mass Measurement
995 (±10 ppm) in Protein Identification Strategies Employing MS or MS/MS and Database Searching.
996 Anal. Chem. *71*, 2871–2882. https://doi.org/10.1021/ac9810516.

997